Journal of Inorganic Biochemistry 269 (2025) 112898

Contents lists available at ScienceDirect

Journal of Inorganic Biochemistry

journal homepage: www.elsevier.com/locate/jinorgbio

Synthesis, structural analysis, and systematic exploration of the antitumor activities of triphenyltin(IV) 2-hydroxy-5-(phenyldiazenyl)benzoates through the modulation of trifluoromethyl variants

Tushar S. Basu Baul [a,*], Amon Das [a], Rupen Tamang [b], Andrew Duthie [c], Biplob Koch [b,*], Sean Parkin [d,*]

[a] Centre for Advanced Studies in Chemistry, North-Eastern Hill University, NEHU Permanent Campus, Umshing, Shillong 793 022, India
[b] Genotoxicology and Cancer Biology Laboratory, Department of Zoology, Institute of Science, Banaras Hindu University, Varanasi 221005, India
[c] School of Life & Environmental Science, Deakin University, Pigdons Road, Waurn Ponds, Victoria 3216, Australia
[d] Department of Chemistry, University of Kentucky, 506 Library Drive, 146 Chemistry-Physics Building, Lexington, KY 40506-0055, USA

ARTICLE INFO

Keywords:
Organotins
Salicylates
Spectroscopy
Crystal structure
Anti-proliferative effects

ABSTRACT

By reacting 5-[(*E*)-2-(2-trifluoromethylphenyl)-1-diazenyl]-2-hydroxybenzoic acid (H′HL^3), 5-[(*E*)-2-(3-trifluoromethylphenyl)-1-diazenyl]-2-hydroxybenzoic acid (H′HL^4), and 5-[(*E*)-2-(4-trifluoromethylphenyl)-1-diazenyl]-2-hydroxybenzoic acid (H′HL^5), with the triphenyltin source Ph_3SnOH, three triphenyltin(IV) 2-hydroxy-5-(phenyldiazenyl)benzoates [$Ph_3Sn(HL^3)$] (**3**), [$Ph_3Sn(HL^4)$] (**4**) and [$Ph_3Sn(HL^5)$] (**5**) were obtained. The resulting tin complexes were characterized using standard spectroscopic techniques and single-crystal X-ray diffraction (SC-XRD). Triphenyltin complexes **3**–**5** exhibit a monomeric distorted tetrahedral configuration, with the fluoro substituted 2-hydroxy-5-(phenyldiazenyl)benzoates coordinating in a monodentate fashion. Additionally, the crystal structure of H′HL^5 is reported. Alongside these, two triphenyltin compounds [$Ph_3Sn(HL^1)$] (**1**) and [$Ph_3Sn(HL^2)$] (**2**), are included to evaluate and compare their anti-proliferative properties. Here, HL^1 and HL^2 represent 5-[(*E*)-2-(phenyl)-1-diazenyl]-2-hydroxybenzoate and 5-[(*E*)-2-(4-fluorophenyl)-1-diazenyl]-2-hydroxybenzoate, respectively. The in vitro antiproliferative activity of the triphenyltin(IV) compounds **1**–**5** was evaluated against MCF-7 (human breast cancer), HeLa (human cervical cancer), and HEK-293 (normal human embryonic kidney) cells and a mechanism of action is proposed on the basis of various biological assays.

1. Introduction

Cancer continues to be a major global health concern and a leading cause of death worldwide. Over the past few decades, the incidence of cancer has steadily increased, with projections estimating that the number of cases will rise from 19.3 million to 28.4 million by 2040 [1,2]. Patients receive tailored therapies such as surgery, chemotherapy, immunotherapy, and radiotherapy based on their cancer type and stage. Chemotherapy, using one or more drugs, has proven effective, but there is a need for new agents that can improve outcomes without harming healthy cells. A notable example is cisplatin, nonetheless, challenges like drug resistance, side effects and ineffective delivery to target sites persist [3–7].

Organotin(IV) carboxylates, represented as $R_{4-n}Sn(OOCR')_n$ (where R, R′ are alkyl or aryl group), are a class of compounds that are formed through the coordination of organotin(IV) species with a variety of carboxylic/benzoic acids. They attain unique stereo electronic configuration leading to the chemical diversity and versatility of tin complexes considering factors like oxidation state, ligand type and number, and coordination geometry. As a result, various organotin complexes have been developed, demonstrating a broad spectrum of applications in catalysis, materials science, biomedicine, optoelectronics, memory devices, photoluminescence, semiconductors, solar cells and dyes in cancer cell detection [8–21]. In the cancer arena, organotins are easily accessible, less toxic than platinum-based drugs, effective at lower doses, which helps reduce resistance and often demonstrate higher activity than cisplatin. This presents an opportunity to develop novel metallopharmaceuticals that can address some of the limitations of current cancer treatments [22–25]. Among non-platinum organometallic chemotherapeutics, tri- and di-organotin compounds, especially

* Corresponding authors.
E-mail address: basubaul@nehu.ac.in (T.S. Basu Baul).

https://doi.org/10.1016/j.jinorgbio.2025.112898
Received 14 January 2025; Received in revised form 25 February 2025; Accepted 13 March 2025
Available online 15 March 2025

carboxylates/benzoates, show promise as anticancer agents against tumor cells compared to currently approved drugs [26–28]. The biological efficiency of organotin(IV) compounds is influenced by the nature of the R group and the ligand (L), typically following this order: $R_3SnL > R_2SnL_2 > RSnL_3 > R_4Sn$ (R = alkyl or aryl, L = mono-anionic ligand) [23,29]. Accordingly, several triphenyltin salicylates were synthesized [30–32] and tested against human breast cancer (MCF-7) and colon cancer (WiDr) cell lines, yielding results comparable to mitomycin C [32]. The coordination ability of 5-[(*E*)-2-(aryl)-1-diazenyl]-2-hydroxybenzoic acid with triorganotin(IV) centers is now established. In the solid state, the trimethyltin complex $[Me_3Sn(HL^{4\text{-}Me})]_n$ forms a one-dimensional polymer with benzoate ligands bridging adjacent Sn centers. The Sn atom adopts a trigonal bipyramidal geometry, with methyl ligands in the equatorial plane and an O atom from a benzoate and a hydroxy O atom from an adjacent ligand in the axial positions. In contrast, the triethyltin complex $[Et_3Sn(HL^{4\text{-}Me})(OH_2)]$ exists as a monomer, featuring a slightly distorted trigonal bipyramidal coordination, with three ethyl ligands in equatorial positions and an O atom from water and a benzoate O atom in the axial positions [33]. Both tribenzyltin $[Bz_3Sn(HL^{4\text{-}Me})]$ and triphenyltin $[Ph_3Sn(HL^{4\text{-}Me})]$ complexes exhibit distorted tetrahedral geometries [33,34]. In all of the above complexes, $HL^{4\text{-}Me}$ refers to 5-[(*E*)-2-(4-methylphenyl)-1-diazenyl]-2-hydroxybenzoates. Five additional triphenyltin(IV) based complexes also exhibit four-coordinate Sn atoms with a similar distorted tetrahedral geometry, using analogues of the ligand with $HL^{2\text{-}Me}$, $HL^{3\text{-}Me}$, $HL^{4\text{-}OMe}$ and $HL^{4\text{-}Cl}$ substitutions [35,36]. Recently, triphenyltin 5-[(*E*)-2-(4-fluorophenyl)-1-diazenyl]-2-hydroxybenzoate, $[Ph_3Sn(HL^{4\text{-}F})]$ was synthesized, tested *in vitro* against prostate cancer cells (DU-145 cell line) and demonstrated strong activity (IC_{50} value of 1.99 ± 0.18 μM) [37].

Given the synthetic and structural significance, along with the potential biological activity of triphenyltin(IV) complex $[Ph_3Sn(HL^{4\text{-}F})]$ [37], it is crucial to further investigate the chemistry of triphenyltin 5-[(*E*)-2-(aryl)-1-diazenyl]-2-hydroxybenzoates, particularly with increased fluorine substitution in the diazo-formed aryl moiety. In this paper, we present the synthesis, spectroscopic analysis, and crystal structures of three $[Ph_3Sn(HL^3)]$ (**3**), $[Ph_3Sn(HL^4)]$ (**4**) and $[Ph_3Sn(HL^5)]$ (**5**) complexes with varying fluoro-substituted ligands: $H'HL^3$ (2-CF_3), $H'HL^4$ (3-CF_3) and $H'HL^5$ (4-CF_3), while the Ph_3Sn moiety is held constant. Additionally, the crystal structure of $H'HL^5$ is reported. For convenience of discussion and comparison, relevant data on structurally characterized triphenyltin 5-[(*E*)-2-(phenyl)-1-diazenyl]-2-hydroxybenzoate $[Ph_3Sn(HL^1)]$ **1** (with no fluorine) and triphenyltin 5-[(*E*)-2-(4-fluorophenyl)-1-diazenyl]-2-hydroxybenzoate $[Ph_3Sn(HL^2)]$ **2** (with one fluorine atom) have been included.

The *in vitro* antiproliferative activity of the triphenyltin(IV) 2-hydroxy-5-(phenyldiazenyl)benzoates **1**–**5** was evaluated against MCF-7 (human breast cancer), HeLa (human cervical cancer), and HEK-293 (normal human embryonic kidney) cells using MTT (3-(4,5-dimethylthiazol-2-yl)-2,5-diphenyltetrazolium bromide) assays. The mechanism of action of the novel triphenyltin(IV) compound $[Ph_3Sn(L^4H)]$ **4** on MCF-7 cells was evaluated through various experiments involving dichlorodihydro-fluorescein diacetate (DCFH-DA), acridine orange and ethidium bromide (AO/EB), along with assessments of mitochondrial dynamics and distribution. Flow cytometry was also utilized to explore the mechanisms behind the drug-induced cytotoxicity. To assess the influence of fluorine in compounds **3**–**5**, the results were compared with those of the non-fluorinated analog **1** and a 4-fluoro compound **2**.

2. Experimental

2.1. Materials and physical measurements

4-Fluoroaniline (Spectrochem), 2-(trifluoromethyl)aniline, 3-(trifluoromethyl)aniline (Sigma-Aldrich), 4-(trifluoromethyl)aniline (Sigma-Aldrich), salicylic acid (Merck) and triphenyltin hydroxide (Alfa Aesar) were utilized as received without additional purification, while aniline was distilled prior to use. Solvents utilized in the reactions were of analytical reagent grade and dried following standard protocols. Toluene and hexane were distilled over benzophenone/sodium, while methanol was distilled over activated magnesium.

For the biological studies, 12-well cell culture plates, 6-well culture plates, Dulbecco's modified eagle medium (DMEM), fetal bovine serum (FBS), penicillin-streptomycin solution, and trypsin-EDTA were obtained from Cell clone while 96 well plates and T-25 cell culture flasks were procured from Eppendorf. MTT (Himedia), dimethyl sulphoxide, DMSO (Merck), DCFH-DA (Sigma-Aldrich), propidium iodide, PI (SRL), acridine orange, AO (Real gene), and ethidium bromide, EB (Loba Chemie), cisplatin (*cis*-diamminedichloroplatinum(II); CDDP), and other analytical grade chemicals were used.

Melting points were determined using a Büchi M-560 melting point apparatus and are uncorrected. Elemental analyses were performed using a Perkin Elmer 2400 series II instrument. The Fourier Transform infrared (FT-IR) spectra of the pro-ligands ($H'HL^1$, $H'HL^2$, $H'HL^3$, $H'HL^4$ and $H'HL^5$) and compounds **1**–**5** were recorded in the range of 400 to 4000 cm^{-1} using a PerkinElmer Spectrum Two spectrometer equipped with UATR accessories, with a resolution of 0.5 cm^{-1}. Solution ^1H (400.13 MHz), ^{13}C (100.62 MHz), ^{19}F (376.3 MHz) and ^{119}Sn (149.15 MHz) nuclear magnetic resonance (NMR) spectra were recorded in $CDCl_3$ and/or DMSO-d_6 as noted, using JEOL Zeta ECZ 400R and Bruker Avance II 400, AMX 400 or Avance IV 400 spectrometers. ^1H, ^{13}C, ^{19}F and ^{119}Sn chemical shifts were referenced to Me_4Si (δ 0.00 ppm), $CDCl_3$ (δ 77.00 ppm), $CFCl_3$ (δ 0.00 ppm) and Me_4Sn (δ 0.00 ppm), respectively. High-resolution mass spectra (HRMS) of compounds **1**–**5** were acquired on a Waters Xevo G2-XS QTOF mass spectrometer employing electrospray ionization. Absorption measurements of pro-ligands ($H'HL^1$, $H'HL^2$, $H'HL^3$, $H'HL^4$ and $H'HL^5$) and compounds **1**–**5** were conducted using an Agilent Technologies Cary 60 spectrophotometer at ambient temperature in freshly prepared DMSO solution (spectroscopy grade, Merck). For the biological studies, a microplate reader (Biorad) and inverted fluorescence microscopes (Evos FL, Life technologies, AMF4300) were used. Crystallographic details are given below.

2.2. Synthesis of the pro-ligands

2.2.1. Synthesis of 5-[(E)-2-(phenyl)-1-diazenyl]-2-hydroxybenzoic acid ($H'HL^1$)

The pro-ligand, $H'HL^1$ was prepared using a diazo-coupling reaction between benzenediazonium chloride and salicylic acid in an alkaline solution under cold conditions, following the method described in earlier reports [35]. However, analytical and spectroscopic data were revisited. The crude product was recrystallized from methanol to yield yellow microcrystalline product. Yield: 1.5 g (23 %). M.p.: 221–222 °C (212–214 °C [35]). FT-IR (ATR mode; ν in cm^{-1}): 3227 (w,br) $\nu(OH)_{phenolic}$, 2853 (w,br) $\nu(OH)_{carboxylic}$, 1661 (vs) $\nu_{as}(OCO)$, 1615 (w), 1446 (vs), 1312 (m), 1223 (s), 1198 (vs), 908 (m), 850 (m), 792 (s), 768 (s), 696 (vs), 683 (vs), 644 (w), 572 (s), 506 (m), 468 (s). ^1H NMR (DMSO-d_6): δ = 8.28 (d, *J* 2 Hz, 1H, H-6), 8.02 (dd, *J* 2 and 9 Hz, 1H, H-4), 7.81 (d, 2H, H-2′ and H-6′), 7.51 (m, 3H, H-3′, H-5′ and H-4), 7.10 (d, *J* 9 Hz, 1H, H-3) ppm. Signals for the phenol and carboxylic acid not observed due to exchange with water in the solvent. ^{13}C NMR ($CDCl_3$/DMSO-d_6): δ = 172.03 (CO_2H), 163.88 (C-2), 151.92 (C-1′), 144.63 (C-5), 130.20 (C-4′), 128.60 (C-3′ and C-5′), 127.86 (C-4), 126.95 (C-6), 122.11 (C-2′ and C-6′), 117.64 (C-3), 112.63 (C-1) ppm. Electronic absorption data (DMSO, λ_{max}[nm]; ε(M^{-1} cm^{-1}): 372, 4680.

2.2.2. Synthesis of 5-[(E)-2-(4-fluorophenyl)-1-diazenyl]-2-hydroxybenzoic acid ($H'HL^2$)

The pro-ligand, $H'HL^2$ was prepared using a diazo-coupling reaction between 4-fluorobenzenediazonium chloride and salicylic acid in an alkaline solution under cold conditions, following the method described in earlier reports [37,38]. The crude product was recrystallized from

methanol, affording a yellow microcrystalline product. Yield: 2.5 g (42 %). M.p.: 250–251 °C (235–236 °C [38]). Anal. found: C, 60.35; H, 3.56; N, 10.66. Calcd. for $C_{13}H_9FN_2O_3$: C, 60.00; H, 3.49; N, 10.77 %. FT-IR (ATR mode; ν in cm^{-1}): 3184 (w, br) $\nu(OH)_{phenolic}$, 2857 (w, br) $\nu(OH)_{carboxylic}$, 1666 (s) $\nu_{as}(OCO)$, 1591 (m), 1447 (s), 1307 (w), 1246 (m), 1205 (vs) ν(C—F), 1135 (m), 1090 (w), 838 (vs), 793 (s), 684 (s), 567 (vs), 514 (w), 468 (vs). Electronic absorption data (DMSO, λ_{max}[nm]; $\varepsilon(M^{-1}\ cm^{-1})$): 372, 3350.

2.2.3. Synthesis of 5-[(E)-2-(2-trifluoromethylphenyl)-1-diazenyl]-2-hydroxybenzoic acid ($H'HL^3$)

2-Trifluromethylaniline (2.5 g, 15.51 mmol) dissolved in a solution of concentrated HCl (8 mL) and water (8 mL) was digested on a water bath for 30 min. The hydrochloride was cooled to −5 °C and diazotized with ice-cold aqueous $NaNO_2$ solution (1.07 g, 15.51 mmol in 5 mL of water). The cold diazonium salt solution was added to salicylic acid (2.14 g, 15.51 mmol) previously dissolved in aqueous NaOH (2.50 g, 62.50 mmol, 25 mL) solution and kept at −5 °C in an ice-salt bath, with vigorous stirring. A light yellow precipitate developed almost immediately, but the stirring was continued for 2 h. The reaction mixture was kept overnight at 4 °C in a refrigerator and on the following day the reaction mixture was allowed to warm to room temperature, whereupon a yellow precipitate separated out. The precipitate was filtered, washed repeatedly with hot water until the pH was neutral and dried in air. The air-dried sample was treated with anhydrous methanol to remove traces of associated water and dried in vacuo. The crude product was boiled thoroughly with hexane, filtered and the residue crystallized with toluene to obtain an orange crystalline material. Yield: 1.1 g, (22 %). M. p.: 215–216 °C. Anal. found: C, 54.55; H, 3.16; N, 9.38. Calcd. for $C_{14}H_9F_3N_2O_3$: C, 54.20; H, 2.92; N, 9.03 %. FT-IR (ATR mode; ν in cm^{-1}): 3146 (w, br) $\nu(OH)_{phenolic}$, 2821 (w, br) $\nu(OH)_{carboxylic}$, 1667 (vs) $\nu_{as}(OCO)$, 1574 (w), 1447 (s), 1313 (s), 1267 (w) ν(C—F), 1173 (m), 1130 (vs), 1054 (s), 904 (w), 838 (w), 766 (s), 698(m), 657 (s), 572 (m), 468 (m). ^{1}H NMR (1:1; $CDCl_3$/DMSO-d_6): δ = 11.89 (br s, 1H, OH), 8.40 (s, 1H, H-6), 8.01 (d, J 9 Hz, 1H, H-4), 7.83 (d, 1H, H-3′), 7.78 (d, 1H, H-6′), 7.71 (t, 1H, H-5′), 7.61 (t, 1H, H-4′), 7.09 (d, 9 Hz, 1H, H-3) ppm. Signals for the carboxylic acid proton were not observed due to exchange with water in the solvent. ^{13}C NMR ($CDCl_3$/DMSO-d_6): δ = 171.79 (CO_2H), 164.52 (C-2), 148.72 (C-1′), 144.70 (C-5), 132.10 (C-5′), 129.54 (C-4′), 128.72 (C-6), 127.31 (C-4), 127.28 (q, ^2J(^{13}C—^{19}F) 31 Hz, C-2′), 125.87 (q, ^3J(^{13}C-^{19}F) 5 Hz, C-3′), 123.46 (q, ^1J(^{13}C-^{19}F) 275 Hz, CF_3), 117.84 (C-3), 115.64 (C-6′), 112.62 (C-1) ppm. ^{19}F NMR ($CDCl_3$); δ = −56.8 ppm. Electronic absorption data (DMSO, λ_{max}[nm]; $\varepsilon(M^{-1}\ cm^{-1})$): 390, 5980.

2.2.4. Synthesis of 5-[(E)-2-(3-trifluoromethylphenyl)-1-diazenyl]-2-hydroxybenzoic acid, ($H'HL^4$)

An analogous method to that used for the preparation of $H'HL^3$ was followed using 3-trifluromethylaniline (2.5 g, 15.51 mmol) and salicylic acid (2.14 g, 15.51 mmol). The yellow precipitated was isolated following the work up procedure described for $H'HL^3$ and recrystallized from toluene to yield a yellow solid. Yield: 1.5 g (31 %). M.p.: 199–200 °C. Anal. found: C, 54.52; H, 2.76; N, 9.30. Calcd. for $C_{14}H_9F_3N_2O_3$: C, 54.20; H, 2.92; N, 9.03 %. FT-IR (ATR mode; ν in cm^{-1}): 3078 (w, br) $\nu(OH)_{phenolic}$, 2873 (w, br) $\nu(OH)_{carboxylic}$, 1668 (vs) $\nu_{as}(OCO)$, 1574 (w), 1433 (w), 1323 (s), 1281 (w), 1209 (m) ν(C—F), 1167 (s), 1141 (vs), 1059 (m), 839 (m), 806 (m), 754 (w), 688 (s), 663 (s), 559 (m), 467 (m). ^{1}H NMR ($CDCl_3$): δ = 10.90 (s, 1H, OH), 8.51 (s, 1H, H-6), 8.11 (d, 1H, H-4), 8.10 (s, 1H, H-2′), 8.02 (d, 1H, H-6′), 7.65 (d, 1H, H-4′), 7.58 (dd, 1H, H-5′), 7.17 (toluene), 7.11 (toluene), 7.08 (d, 9 Hz, 1H, H-3), 2.28 (toluene) ppm. Signals for the carboxylic acid proton were not observed due to exchange with water in the solvent. ^{13}C NMR ($CDCl_3$/DMSO-d_6): δ = 171.17 (CO_2H), 163.77 (C-2), 151.16 (C-1′), 143.59 (C-5), 130.06 (q, ^2J(^{13}C-^{19}F) 33 Hz, C-3′), 128.85 (C-5′), 127.88 (toluene), 127.32 (C-4), 127.10 (toluene), 126.86 (toluene), 126.76 (C-6), 125.68 (q, ^3J(^{13}C-^{19}F) 3 Hz), 125.22 (C-6′), 122.80 (q, ^1J(^{13}C-^{19}F) 272 Hz, CF_3), 117.78 (^3J(^{13}C-^{19}F) 4 Hz, C-2′), 117.17 (C-3), 112.16 (C-1) ppm. ^{19}F NMR ($CDCl_3$); δ = −62.0 ppm. Electronic absorption data (DMSO, λ_{max}[nm]; $\varepsilon(M^{-1}\ cm^{-1})$): 383, 5212.

2.2.5. Synthesis of 5-[(E)-2-(4-trifluoromethylphenyl)-1-diazenyl]-2-hydroxybenzoic acid, ($H'HL^5$)

An analogous method to that used for the preparation of $H'HL^3$ was followed using 4-trifluromethylaniline (2.5 g, 15.51 mmol) and salicylic acid (2.14 g, 15.51 mmol). The yellow precipitated was isolated following the work up procedure described for $H'HL^3$ and recrystallized from methanol to yield a yellow solid. Yield: 1.60 g (33 %). M.p.: 237–238 °C. Anal. found: C, 54.55; H, 2.76; N, 9.55. Calcd. for $C_{14}H_9F_3N_2O_3$: C, 54.20; H, 2.92; N, 9.03 %. FT-IR (ATR mode; ν in cm^{-1}): 3065 (w, br) $\nu(OH)_{phenolic}$, 2868 (w, br) $\nu(OH)_{carboxylic}$, 1664 (vs) $\nu_{as}(OCO)$, 1450 (s), 1317 (vs), 1202 (s) ν(C—F), 1162 (s), 1122 (vs), 1062 (vs), 844 (vs), 796 (w), 696 (vs), 599 (m), 563 (w), 464 (w). ^{1}H NMR ($CDCl_3$): δ = 11.00 (s br, 1H, OH), 8.50 (s, 1H, H-6), 8.10 (d, J 9 Hz, 1H, H-4), 7.91 (d, 2H, H-2′), 7.71 (d, 2H, H-3′), 7.08 (d, J 9 Hz, 1H, H-3) ppm. Signals for the carboxylic acid proton were not observed due to exchange with water in the solvent. ^{13}C NMR (DMSO-d_6): δ = 171.32 (CO_2H), 164.31 (C-2), 154.00 (C-1′), 144.39 (C-1), 130.45 (q, ^2J (^{13}C-^{19}F) 32 Hz, C-4′), 129.12 (C-4), 126.67 (C-6), 126.61 (q, ^3J(^{13}C-^{19}F) 3 Hz, C-3′), 123.00 (C-2′), 118.58 (C-3), 113.87 (C-5) ppm. ^{19}F NMR ($CDCl_3$); δ = −62.5 ppm. Electronic absorption data (DMSO, λ_{max}[nm]; $\varepsilon(M^{-1}\ cm^{-1})$): 389, 6246.

2.3. Synthesis of triphenyltin(IV) compounds

2.3.1. Synthesis of $[Ph_3Sn(HL^1)]$ (1)

Compound $[Ph_3Sn(HL^1)]$ **1** was previously synthesized by reacting $NaHL^1$ with Ph_3SnCl in methanol [35]. In the current study, compound **1** was produced by reacting $H'HL^1$ (0.25 g, 1.03 mmol) with Ph_3SnOH (0.378 g, 1.03 mmol) in 40 mL of anhydrous toluene, utilizing a Dean-Stark moisture trap and a water-cooled condenser. The reaction mixture was refluxed for 6 h and filtered. The resulting clear orange solution was evaporated to dryness using a rotary evaporator and subsequently dried under vacuum. The solid was then triturated with hexane (5 × 0.5 mL), and the dried residue dissolved in a larger volume of hexane (30 mL) and filtered. The filtrate, upon evaporation, yielded orange crystals of the desired product. Yield: 0.34 g (55 %). M. p.: 141–142 °C (136–138 °C [35]). Anal. found: C, 63.29; H, 3.87; N, 4.61. Calcd. for $C_{31}H_{24}N_2O_3Sn$: C, 62.97; H, 4.09; N, 4.74 %. FT-IR (ATR mode; ν in cm^{-1}): 3051 (w, br) $\nu(OH)_{phenolic}$, 1633 (vs) $\nu_{as}(OCO)$, 1589 (s), 1415 (s), 1370 (vs), 1299 (s), 1235 (s) ν(C—F), 1077 (s), 997 (w), 922 (w), 767 (w), 726 (vs), 688 (vs) ν(Sn—C), 610 (w), 571 (w), 508 (w), 444 (vs), 424 (s). ^{1}H NMR ($CDCl_3$): δ = 11.51 (s, 1H, OH), 8.54 (d, J 2 Hz, 1H, H-6), 7.97 (dd, J 2 and 9 Hz, 1H, H-4), 7.80 (d, 2H, H-2′ and H-6′), 7.73 (m, 6H, Ph-2), 7.42 (m, 12H, H-3′, H-5′, H-4, Ph-3 and Ph-4), 6.98 (d, J 9 Hz, 1H, H-3) ppm. ^{13}C NMR ($CDCl_3$): δ = 174.70 (CO_2), 164.11 (C-2), 152.56 (C1′), 145.26 (C-5), 137.32 (Ph-1), 136.86 (^2J (^{13}C-$^{117/119}$Sn) 48 Hz, Ph-2), 130.55 (^4J(^{13}C-$^{117/119}$Sn) 13 Hz, Ph-4), 129.25 (C-4), 129.12 (^3J(^{13}C-$^{117/119}$Sn) 62/65 Hz, Ph-3), 129.03 (C-3′ and C-5′), 127.61 (C6), 122.58 (C-2′ and C-6′), 118.07 (C-3), 113.59 (C-1) ppm. ^{119}Sn NMR ($CDCl_3$); δ = −88.8 ppm [35]. Electronic absorption data (DMSO, λ_{max}[nm]; $\varepsilon(M^{-1}\ cm^{-1})$): 376, 2456.

2.3.2. Synthesis of $[Ph_3Sn(HL^2)]$ (2)

An analogous method to that used for preparing compound **1** was employed, utilizing Ph_3SnOH (0.35 g, 0.96 mmol) and $H'HL^2$ (0.25 g, 0.96 mmol). After the workup, the residue was extracted by boiling it in a large volume of hexane (30 mL) and then filtered. To this, 2 mL of ethanol was added, and upon evaporation at room temperature, orange crystals of compound **2** were obtained. Yield: 0.35 g (60 %). M. p.: 143–144 °C. Anal. found: C, 60.95; H, 3.44; N, 4.70. Calcd. for $C_{31}H_{23}FN_2O_3Sn$: C, 61.12; H, 3.81; N, 4.60 %. FT-IR (ATR mode; ν in cm^{-1}): 3056 (w, br) ν(O—H)$_{phenolic}$, 1623 (vs) $\nu_{as}(OCO)$, 1589 (m), 1480

(m), 1431 (w), 1296 (w), 1250 (w), 1217 (w) ν(C—F), 1076 (m), 997 (w), 841 (s), 801 (m), 777 (w), 726 (vs), 693 (vs) ν(Sn—C), 571 (s), 443 (vs). ^{1}H NMR ($CDCl_3$); $\delta = 11.54$ (s, 1H, OH), 8.51 (d, *J* 2 Hz, 1H, H-6), 7.95 (dd, *J* 2 and 9 Hz, 1H, H-4), 7.81 (m, 2H, H-2′ and H-6′), 7.74 (m, 6H, Ph-2), 7.44 (m, 9H, Ph-3 and Ph-4), 7.10 (t, 2H, H-3′, H-5′), 6.97 (d, *J* 9 Hz, 1H, H-3) ppm. ^{13}C NMR ($CDCl_3$) $\delta = 174.62$ (CO_2), 164.11 (C-2), 164.04 (d, ^{1}J(^{13}C-^{19}F) 252 Hz, C-4′), 149.06 (d, ^{4}J(^{13}C-^{19}F) 3 Hz, C-1′), 145.05 (C-1), 137.43 (Ph-1), 136.86 (^{2}J(^{13}C-$^{117/119}$Sn) 49 Hz, Ph-2), 130.53 (^{4}J(^{13}C-$^{117/119}$Sn) 15 Hz, Ph-4), 129.16 (C-4), 129.11 (^{3}J(^{13}C-$^{117/119}$Sn) 64 Hz, Ph-3), 127.53 (C-6), 124.52 (d, ^{3}J(^{13}C-^{19}F) 8 Hz, C-2′), 118.08 (C-3), 115.96 (d, ^{2}J(^{13}C-^{19}F) 23 Hz, C-3′) 113.71 (C-5) ppm. ^{19}F NMR ($CDCl_3$); $\delta = -109.9$ ppm. ^{119}Sn NMR ($CDCl_3$); $\delta = -88.1$ ppm. Electronic absorption data (DMSO, λ_{max}[nm]; ε(M^{-1} cm^{-1}): 375, 1923.

2.3.3. Synthesis of [$Ph_3Sn(HL^3)$] (3)

An analogous method to that used for the preparation of **1** was followed using Ph_3SnOH (0.295 g, 0.80 mmol) and H′HL^3 (0.25 g, 0.80 mmol). After workup, the orange residue was extracted by boiling it in a large volume of hexane (30 mL) and then filtered. To this, 2 mL of ethanol was added, and upon evaporation at room temperature, orange crystals of compound **3** were obtained. Yield: 0.31 g (58 %). M. p: 183–184 °C. Anal. found: C, 58.09; H, 3.44; N, 4.09. Calcd. for $C_{32}H_{23}F_3N_2O_3Sn$: C, 58.30; H, 3.52; N, 4.25 %. FT-IR (ATR mode; *ν* in cm^{-1}): 3050 (w, br) ν(O—H)$_{phenolic}$, 1633 (vs) ν_{as}(OCO), 1591 (m), 1482 (w), 1417 (w), 1392 (m), 1314 (m), 1254 (m), 1238 (m) ν(C—F), 1175 (m), 1130 (vs), 1075 (m), 1052 (w), 997 (w), 918 (w), 806 (s), 764 (s), 729 (vs), 695 (s) ν(Sn—C), 659 (s), 573 (m) 538 (m), 446 (vs). ^{1}H NMR ($CDCl_3$): $\delta = 11.62$ (s, 1H, OH), 8.63 (d, *J* 2 Hz, 1H, H-6), 8.01 (dd, 1H, H-4), 7.74 (m, 8H, H-3′, H-6′ and Ph-2), 7.56 (t, 1H, H-5′), 7.44 (m, 10H, H-4′, Ph-3 and Ph-4) 6.99 (d, *J* 9 Hz, 1H, H-3) ppm. ^{13}C NMR (DMSO-d_6): $\delta = 174.50$ (CO_2), 164.73 (C-2), 149.39 (C-1′), 145.42 (C-5), 137.17 (Ph-1), 136.86 (^{2}J(^{13}C-$^{117/119}$Sn) 48 Hz, Ph-2), 132.50 (C-5′), 130.58 (^{4}J(^{13}C-$^{117/119}$Sn) 14 Hz, Ph-4), 129.92 (C-4′), 129.32 (C-6), 129.14 (^{3}J(^{13}C-$^{117/119}$Sn) 64 Hz, Ph-3), 128.91 (C-4), 128.16 (q, ^{2}J(^{13}C-^{19}F) 31 Hz, C-2′), 126.58 (q, ^{3}J(^{13}C-^{19}F) 5 Hz, C3′), 124.07 (q, ^{1}J(^{13}C-^{19}F) 274 Hz, CF_3), 118.20 (C-3), 116.09 (C-6′), 113.81 (C-1). ^{19}F NMR ($CDCl_3$); $\delta = -57.6$ ppm. ^{119}Sn NMR ($CDCl_3$); $\delta = -90.3$ ppm. Electronic absorption data (DMSO, λ_{max}[nm]; ε(M^{-1} cm^{-1}): 392, 1416.

2.3.4. Synthesis of [$Ph_3Sn(HL^4)$] (4)

An analogous method to that used for the preparation of **1** was followed using Ph_3SnOH (0.295 g, 0.80 mmol) and H′HL^4 (0.25 g, 0.80 mmol). After workup, the orange residue was extracted by boiling it in a large volume of hexane (30 mL) and then filtered. To this, 2 mL of ethanol was added, and upon evaporation at room temperature, orange crystals of compound **4** were obtained. Yield: 0.34 g (64 %). M. p: 120–121 °C. Anal. found: C, 58.75; H, 3.44; N, 4.66. Calcd. for $C_{32}H_{23}F_3N_2O_3Sn$: C, 58.30; H, 3.52; N, 4.25 %. FT-IR (ATR mode; *ν* in cm^{-1}): 3054 (w, br) ν(O—H)$_{phenolic}$, 1633 (vs) ν_{as}(OCO), 1591 (vs), 1591 (vs), 1481 (w), 1418 (s), 1399 (m), 1329 (s), 1254 (s) ν(C—F), 1239 (w), 1169 (s), 1127 (vs), 1063 (w), 997 (w), 914 (m), 842 (m), 805 (s), 764 (w), 732 (vs), 691 (vs) ν(Sn—C), 662 (m), 568 (m) 508 (m), 447 (vs). ^{1}H NMR ($CDCl_3$): $\delta = 11.69$ (s, 1H, OH), 8.65 (d, *J* 2 Hz, 1H, H-6), 8.15 (s, 1H, H-2′), 8.07 (m, 2H, H-4 and H-6′), 7.82 (m, 6H, Ph-2), 7.70 (d, *J* 2 and 9 Hz, 1H, H-4′), 7.63 (dd, 1H, H-5′), 7.53 (m, 9H, Ph-3 and Ph-4), 7.07 (d, 1H, H-3) ppm. ^{13}C NMR ($CDCl_3$): $\delta = 174.60$ (CO_2), 164.66 (C-2), 152.47 (C-1′), 144.95 (C-5), 137.21 (Ph-1), 136.88 (^{2}J(^{13}C-$^{117/119}$Sn) 48 Hz, Ph-2), 131.56 (^{2}J(^{13}C-^{19}F) 33 Hz, C-3′), 130.61 (^{4}J(^{13}C-$^{117/119}$Sn) 14 Hz, Ph-4), 129.88 (C-6), 129.62 (C-5′), 129.15 (^{3}J(^{13}C-$^{117/119}$Sn) 62/65 Hz, Ph-3), 128.31 (benzene), 127.60 (C-4), 126.74 (^{3}J(^{13}C-^{19}F) 3 Hz, C-4′), 126.12 (C-6′), 123.85 (^{1}J(^{13}C-^{19}F) 272 Hz, CF_3), 119.19 (^{3}J(^{13}C-^{19}F) 4 Hz, C-2′), 118.24 (C-3), 113.71 (C-1) ppm. ^{19}F NMR ($CDCl_3$); $\delta = -62.6$ ppm. ^{119}Sn NMR ($CDCl_3$); $\delta = -90.9$ ppm. Electronic absorption data (DMSO, λ_{max}[nm]; ε(M^{-1} cm^{-1}): 387, 1626.

2.3.5. Synthesis of [$Ph_3Sn(HL^5)$] (5)

An analogous method to that used for the preparation of **1** was followed using Ph_3SnOH (0.295 g, 0.80 mmol) and H′HL^5 (0.25 g, 0.80 mmol). After workup, the red-orange residue was extracted by boiling in large volume of hexane and filtered. Ethanol was added (10:1, v/v), which upon evaporation at room temperature yielded red-orange crystals of **5** suitable for diffraction studies. Yield: 0.33 g (62 %). M. p: 179–180 °C. Anal. found: C, 58.03; H, 3.54; N, 4.55. Calcd. for $C_{32}H_{23}F_3N_2O_3Sn$: C, 58.30; H, 3.52; N, 4.25 %. FT-IR (ATR mode; *ν* in cm^{-1}): 3069 (w, br) ν(OH)$_{phenolic}$, 1636 (vs) ν_{as}(OCO), 1591 (m), 1481 (m), 1391 (m), 1323 (s), 1302 (s), 1259 (m), 1238 (m), 1174 (s), 1126 (vs) ν(C—F), 1064 (vs), 997 (w), 917 (w), 846 (m), 806 (s), 729(vs), 694 (w) ν(Sn—C), 658 (w), 601 (w), 444 (s). ^{1}H NMR ($CDCl_3$): $\delta = 11.68$ (s, 1H, OH), 8.65 (d, *J* 2 Hz, 1H, H-6), 8.07 (dd, *J* 2 and 9 Hz, 1H, H-4), 7.95 (d, 2H, H-2′), 7.82 (m, 6H, Ph-2), 7.75 (d, 2H, H-3′), 7.51 (m, 9H, Ph-3 and Ph-4), 7.06 (d, *J* 9 Hz, 1H, H-3) ppm. ^{13}C NMR ($CDCl_3$): $\delta = 174.55$ (CO_2), 164.78 (C-2), 154.40 (C-1′), 145.08 (C-1), 137.29 (Ph-1), 136.88 (^{2}J(^{13}C-$^{117/119}$Sn) 48 Hz, Ph-2), 131.68 (q, ^{2}J(^{13}C-^{19}F) 33 Hz, C-4′), 130.60 (Ph-4), 129.98 (C-6), 129.15 (^{3}J(^{13}C-$^{117/119}$Sn) 64 Hz, Ph-3), 127.65(C-4), 126.22 (q, ^{3}J(^{13}C-^{19}F) 2 Hz, C-3′), 122.76 (C-2′), 118.25 (C-3), 113.78 (C-5) ppm. ^{19}F NMR ($CDCl_3$); $\delta = -62.3$ ppm. ^{119}Sn NMR ($CDCl_3$); $\delta = -86.8$ ppm. Electronic absorption data (DMSO, λ_{max}[nm]; ε(M^{-1} cm^{-1}): 391, 1366.

IR (signal intensity): s, strong; vs, very strong; m, medium; w, weak; br, broad.

NMR (signal multiplicity): s, singlet; d, doublet; dd, doublet of doublets; t, triplet; m, multiplet; br, broad.

2.4. X-ray crystallography

Single crystals suitable for X-ray analysis were obtained by slow evaporation using various solvent systems: dimethyl sulfoxide for H′HL^5 and a mixture of hexane/ethanol (2:1, *v*/v) for [$Ph_3Sn(HL^3)$] (**3**), [$Ph_3Sn(HL^4)$] (**4**) and [$Ph_3Sn(HL^5)$] (**5**).

For each sample, a suitable crystal was mounted from oil (polyisobutene) on a fine glass fibre and flash-cooled [39] to either 100 K (for **3**, **4**), 180 K (for H′HL^5, to avoid a destructive phase transition), or 220 K (for **5**, to avoid a low-temperature transition to a modulated structure, though substantial diffuse scatter remained). Diffraction data were collected using a dual-microsource Bruker D8 Venture diffractometer using Mo*Kα* ($\lambda = 0.71073$ Å) or Cu*Kα* ($\lambda = 1.54178$ Å, **4** only) radiation. Data collection and reduction [40], absorption correction [41,42], structure solution [43] refinement [44], and validation [45,46] were by published methods. There was torsional disorder of the CF_3 groups in both H′HL^5 and **5**, while **5** also exhibited extensive disorder of its $SnPh_3$ group.

2.5. Solubility and stability assessment of organotin(IV) compounds 1–5

The organotin(IV) compounds **1**–**5** are soluble in all commonly used solvents, while they exhibit insolubility in water. Ensuring drug stability under physiological conditions is essential for *in vitro* and *in vivo* applications. Organotin(IV) compounds are typically dissolved in DMSO and diluted with a test medium for *in vitro* testing. To assess their stability, the pro-ligands (**H′HL^1**, **H′HL^2**, **H′HL^3**, **H′HL^4** and **H′HL^5**) and their triphenyltin compounds **1**–**5** (compound **4** also in buffer solution at a physiological pH 7.2) were analyzed using UV–visible spectroscopy in DMSO (ESI Figs. S1 and S2) before cytotoxic studies, showing consistent absorption spectra over 21 days [47]. For hydrolytic stability studies, compound **4**, which was identified as the most active compound, was dissolved in DMSO at a concentration of 1×10^{-4} M and then diluted with distilled water to achieve a final concentration of 1×10^{-6} M. UV–Vis spectra were recorded immediately after preparation and at 72 h (i.e., at 0 and 72 h; see ESI Fig. S3). During the investigation period, compound **4** showed no signs of decomposition.

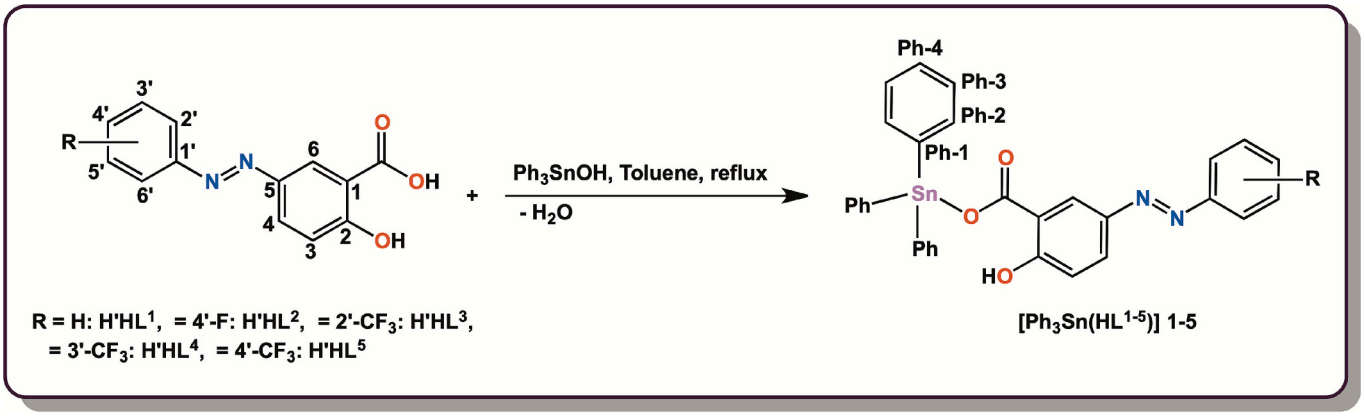

Scheme 1. Reaction scheme showing the preparation of triphenyltin(IV) compounds **1**–**5**, along with atom numbering for the pro-ligands (free acid H′HL$^{1–5}$, where H and H′ represent hydroxyl and carboxylic acid protons, respectively) as well as the *Sn*-phenyl moiety to aid in NMR signal assignments.

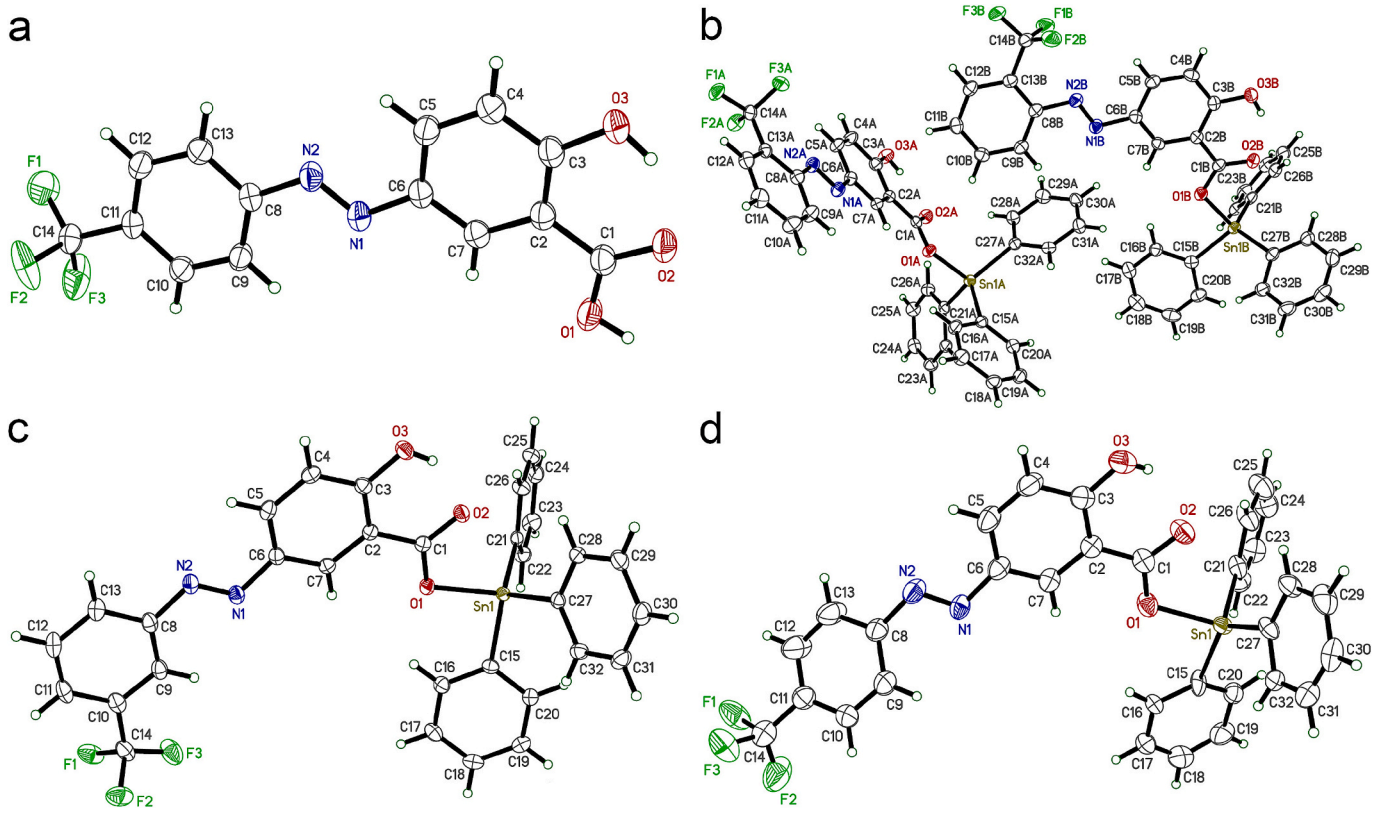

Fig. 1. Ellipsoid plots of (a) H′HL^5, (b) **3**, (c) **4**, and (d) **5**, drawn at 50 % probability for H′HL^5, **3**, **4** and 30 % for **5**. Hydrogen atoms are drawn as small circles of arbitrary size. For the sake of clarity, only the major components of disorder shown for H′HL^5 and **5**.

2.6. Experimental protocol and anti-proliferative activity tests

2.6.1. Cell line culture and experimental setup

MCF-7 (human breast cancer), HeLa (human cervical cancer), and HEK-293 (normal human embryonic kidney) cells were sourced from the National Centre for Cell Science (NCCS) in Pune, India. These cells were cultured in DMEM, supplemented with 10 % heat-inactivated FBS. Penicillin-streptomycin solution were added, and the cells were maintained at 37 °C in a humidified atmosphere with 5 % CO_2. Harvesting occurred when cells reached 80 % confluence, followed by plating for subsequent tests.

The triphenyltin compounds (test compounds) **1**–**5**, pro-ligands (H′HL^1, H′HL^2, H′HL^3, H′HL^4 and H′HL^5) and triphenyltin precursor (reference compound: Ph_3SnOH), were initially prepared in DMSO as 100 mM stock solutions and stored at 4 °C for later use. These stock solutions were then diluted to appropriate working concentrations with DMEM for subsequent experiments, ensuring that the final DMSO concentration did not surpass 0.1 %. The stock solution of CDDP at 1 mM was prepared in a normal saline aqueous solution containing 0.9 % sodium chloride.

2.6.2. Anti-proliferative assays and determination of IC_{50} values

The inhibitory activity of the test compounds was evaluated using the MTT assay, which relies on conversion of the yellow tetrazolium salt to purple formazan by mitochondrial dehydrogenase [48], thus assessing cell viability. Test compounds **1**–**5** were tested for cytotoxicity

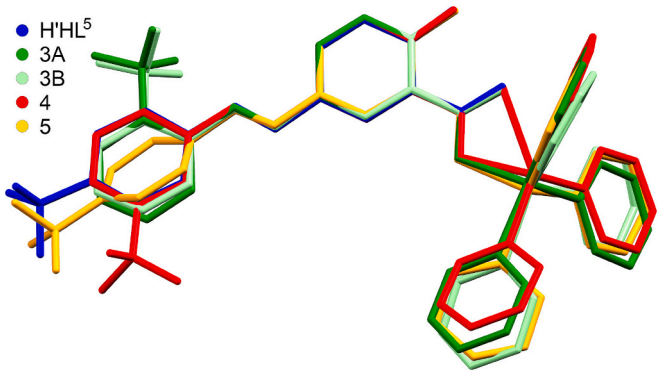

Fig. 2. A least-squares overlay plot of H′HL[5], **3**, **4**, and **5** (structure **3** has two crystallographically distinct molecules, **3A** and **3B**). Minor components of disorder for H′HL[5] and **5** are not shown. For each structure, the fit was through atoms O1-O3,N1,N2,C1-C8. The largest deviation occurs for the $C_6H_4CF_3$ group of **5** (orange).

Table 1
Selected interatomic distances (Å) in compounds H′HL[5], **3**, **4** and **5**.

Distance	H′HL[5]	3A	3B	4	5[a]
Sn1-O1	–	2.0666(16)	2.0654(16)	2.0849(10)	2.145(4)
Sn1-O2[b]	–	2.9003(17)	2.8602(18)	2.7535(11)	3.012(4)
Sn1-C15	–	2.132(2)	2.124(3)	2.1343(15)	2.052(9)
Sn1-C21	–	2.117(2)	2.129(2)	2.1256(15)	2.179(9)
Sn1-C27	–	2.118(2)	2.110(2)	2.1250(15)	2.059(8)
C1-O1	1.305(2)	1.300(3)	1.303(3)	1.2951(18)	1.305(5)
C1-O2	1.235(2)	1.247(3)	1.243(3)	1.2461(18)	1.247(5)
C3-O3	1.347(2)	1.349(3)	1.344(3)	1.3458(18)	1.347(5)
C1-C2	1.463(2)	1.472(3)	1.477(3)	1.478(2)	1.458(6)
N1-C6	1.427(2)	1.420(3)	1.425(3)	1.4267(19)	1.438(5)
N1-N2	1.250(2)	1.255(3)	1.251(3)	1.2574(18)	1.236(4)
N2-C8	1.425(2)	1.430(3)	1.431(3)	1.428(2)	1.422(5)

[a] Major disorder component only.
[b] Sn1-O2 distances are included because O2 influences the geometry at Sn1.

against MCF-7 and HeLa cancer cells, as well as normal HEK-293 cells, at various concentrations. Pro-ligands (H′HL[1], H′HL[2], H′HL[3], H′HL[4] and H′HL[5]) and reference compound (Ph_3SnOH), along with CDDP, were included for comparison. Approximately 1×10^4 cells/well were seeded in three separate sterile 96-well microplates with complete medium and incubated at 37 °C for 24 h to ensure cell adherence.

Subsequently, the cells were treated with varying concentrations (ranging 0.10 to 80 μM for MCF-7 and HeLa, and from 0.10 to 50 μM for HEK-293) of the test compounds, including CDDP. Following this, they were incubated once more at 37 °C for 24 h, after which the exhausted medium was removed. A mixture of 100 μL of freshly prepared MTT solution (derived from a stock solution of 5 mg mL^{-1}) was added to each well, and the cells were incubated again at 37 °C for 2 h. After removing the medium with the MTT solution, 100 μL of DMSO was added to each well to dissolve the insoluble purple MTT formazan crystals. Following a 30 min incubation period, the absorbance of the samples was measured at 570 nm using a microplate reader. All experiments were carried out concurrently and in triplicate. The anti-proliferative activities of both the test and reference compounds are quantified as the percentage of reduced cell growth in treated cells compared to control cells, expressed as Cell viability (%) = Absorbance of treated cells/Absorbance of control cells ×100.

To ascertain the effectiveness of the test compounds, we determined the IC_{50} (inhibitory concentration) value, representing the concentration at which 50 % inhibition of cell growth occurs, was determined and expressed it as the mean ± standard error of the mean (SEM).

Further experiments with the MCF-7 cells were continued because compound **4** proved effective. It demonstrated significant cytotoxicity

Table 2
Selected bond angles, torsions[a], and dihedrals (°) in compounds H′HL[5], **3**, **4** and **5**.

Angle	H′HL[5]	3A	3B	4	5[b]
O1-Sn1-O2[c]	–	49.74(5)	50.59(6)	52.17(4)	47.42 (10)
O1-Sn1-C15	–	95.20(8)	95.38(8)	93.94(5)	95.2(3)
O1-Sn1-C21	–	109.55 (8)	108.31(8)	109.68(5)	101.8(3)
O1-Sn1-C27	–	107.19 (8)	106.92(8)	110.12(5)	103.9(3)
N1-N2-C8	115.61 (14)	113.9(2)	114.0(2)	114.79 (13)	113.4(4)
N2-N1-C6	112.63 (14)	114.1(2)	113.8(2)	112.86 (13)	114.2(4)
O1-C1-C2-C3	179.39 (16)	176.5(2)	176.8(2)	174.72 (13)	179.2(4)
N1-N2-C8-C13	175.85 (15)	176.8(2)	174.7(2)	177.77 (14)	154.4(5)
N2-N1-C6-C7	179.89 (15)	179.6(2)	178.3(2)	179.99 (13)	167.5(4)
C6-N1-N2-C8	178.55 (14)	177.8(2)	179.21 (19)	177.67 (12)	179.8(4)
∠ L_{Mc}-L_{Ph1}	–	6.22(15)	4.07(13)	6.87(10)	3.43(2)
∠ L_{Ph1}-L_{Ph2}	6.61(7)	4.48(16)	9.87(12)	7.57(10)	40.36 (19)

L_{Mc} is the mean plane through atoms Sn1-O1-C1-O2.
L_{Ph1} and L_{Ph2} are mean planes through phenyl rings C2-C7 and C8-C13, respectively.
[a] Absolute values of torsion angles.
[b] Major disorder component only.
[c] O1-Sn1-O2 angles are included because O2 influences the geometry at Sn1.

with minimal effects on normal cells while other test compounds, **1**–**5**, exhibited high cytotoxicity in HeLa cells.

2.6.3. Reactive oxygen species (ROS) generation assay

Elevated levels of ROS show when cells are under stressed conditions. ROS levels can be assessed by treating samples with DCFH-DA and subsequently measuring the fluorescence. The assay was carried out on the most active test compound **4**, to assess its impact on ROS production in MCF-7 and HEK-293 cells [49]. The oxidation-sensitive fluorescent dye DCFH-DA was utilized to examine intracellular ROS levels induced by compound **4** across various concentrations.

For the experiment, MCF-7 and HEK-293 cells (5×10^4) were evenly distributed into two separate sterile 12-well culture plates and then incubated at 37 °C for 24 h. Subsequently, the cells were treated with various concentrations of compound **4** (0.2 μM, 0.4 μM (IC_{50} concentration), and 1 μM). After another 24-h incubation period, both the treated cells and the controls were washed once with phosphate-buffered saline (PBS), followed by exposure to 10 μM of the DCFH-DA dye for 30 min, and then subjected to two additional washes with PBS. The treated cell samples along with the control were subsequently examined to quantify reactive oxygen species levels. This analysis utilized inverted fluorescence microscopy, capturing images in the green channel and in the phase contrast mode. All experiments were carried out simultaneously and in triplicate.

2.6.4. Detection of apoptosis (acridine orange/ethidium bromide AO/EB assay)

The AO/EB dual staining assay offers a method to evaluate the integrity of the cell membrane, enabling the differentiation of early, late, and necrotic cells. This technique involves permeating the cell membrane and dual staining DNA using AO/EB, providing an alternative approach to assess tumor cell apoptosis via fluorescence measurement. AO penetrates the plasma membrane and binds to the DNA of viable cells, emitting a green fluorescence, while EB selectively stains the DNA of dead cells, producing a red-orange fluorescence signal.

For the experiment, MCF-7 and HEK-293 cells (5×10^4 cells per well)

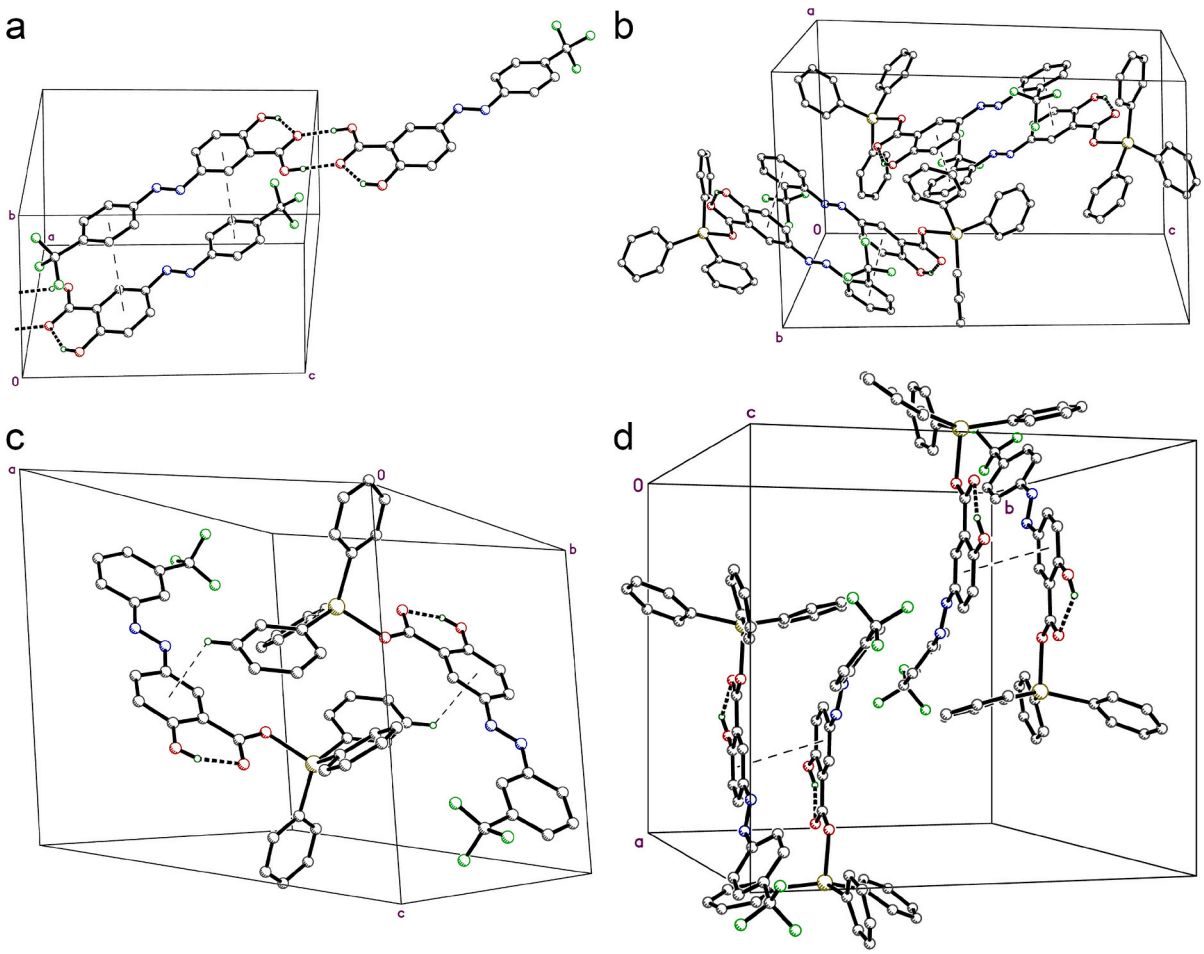

Fig. 3. Partial packing plots of (a) H′HL[5], (b) **3**, (c) **4**, and (d) **5**, showing the most important supramolecular constructs in each structure. Hydrogen bonds are drawn as thick dashed lines, while π… π and C-H… π contacts are shown as thin dashed lines.

Table 3
Relevant hydrogen bonds, π…π, and C-H…π interactions (Å) compounds H′HL[5], **3**, **4**, and **5**.

Interaction	H′HL[5]	3A	3B	4	5[b]
O3—H3… O2	2.6035(19)	2.605(2)	2.611(3)	2.5837(16)	2.596(5)
O1—H1… O2	2.6518(18) [i]	–	–	–	–
*Cg*1…*Cg*2	3.8616 (19)[ii]	3.597 (3)[iii]	3.860 (3)[iv]	–	–
*Cg*1…*Cg*1	–	–	–	–	3.491 (5)[v]
C19…*Cg*1	–	–	–	3.3617 (16)[ii]	–
H19…*Cg*1	–	–	–	2.8871[ii]	–

i = 1-*x*, 2-*y*, 2-*z*; *ii* = 1-*x*, 1-*y*, 1-*z*; *iii* = −*x*, −*y*, −*z*; *iv* = 1-*x*, −*y*, 1-*z*; *v* = 0.5-*x*, 1.5-*y*, *z*.
*Cg*1 = centroid of ring C2-C7; *Cg*2 = centroid of ring C8-C13.

were plated in sterile 12-well culture plates and incubated at 37 °C for 24 h. Following this, the cells were treated with various concentrations of test compound **4** (lower (0.2 μM), IC_{50} (0.4 μM), and higher (1 μM)). After 24 h of treatment, the cells were rinsed with PBS and then stained for 45 min with a solution containing 20 μg/mL AO and 2 μg/mL EB. Following two washes with PBS, the cell samples and controls were examined using inverted fluorescence microscopy (EVOS live cell imaging equipment from Life Technologies), capturing images in the red and green channels. All experiments were carried out simultaneously and at least in triplicate.

2.6.5. Mitochondrial aggregation (Mitotracker)

It has been demonstrated that different anticancer drugs induce apoptosis by modifying the distribution pattern and structure of mitochondria. Moreover, pro-apoptotic signals are associated with these changes in mitochondrial distribution within cells. The observation of mitochondrial fluorescence is typically conducted using MitoTracker, a lipophilic cationic dye that is absorbed by the mitochondria [50].

To evaluate the distribution pattern of mitochondria, 5×10^4 MCF-7 cells were plated in 12-well plates and allowed to incubate overnight. Subsequently, the MCF-7 cells were exposed to different concentrations of test compound **4** (lower (0.2 μM), IC_{50} (0.4 μM), and higher (1 μM)) and further incubated for 24 h. Following this incubation period, the cells were rinsed with PBS and were stained with both Hoechst and Mitotracker for 30 min. Fluorescence microscopy (Evos FL cell imaging system) was employed to capture images of the cells in phase contrast, blue, and red channels.

2.6.6. Cell cycle analysis

Flow cytometry combined with propidium iodide (PI) labeling was employed to assess the impact of test compound **4** on the distribution of MCF-7 cells throughout the cell cycle. Initially, trypsinized cells were plated and allowed to incubate overnight in 6-well plates under humidified conditions. Subsequently, the cells were subjected to treatment with concentrations of (lower (0.2 μM), IC_{50} (0.4 μM), and higher (1 μM)). Following a 24 h treatment period, the cells were harvested using 1.0 mM EDTA, fixed with 75 % ethanol, and then stored overnight at

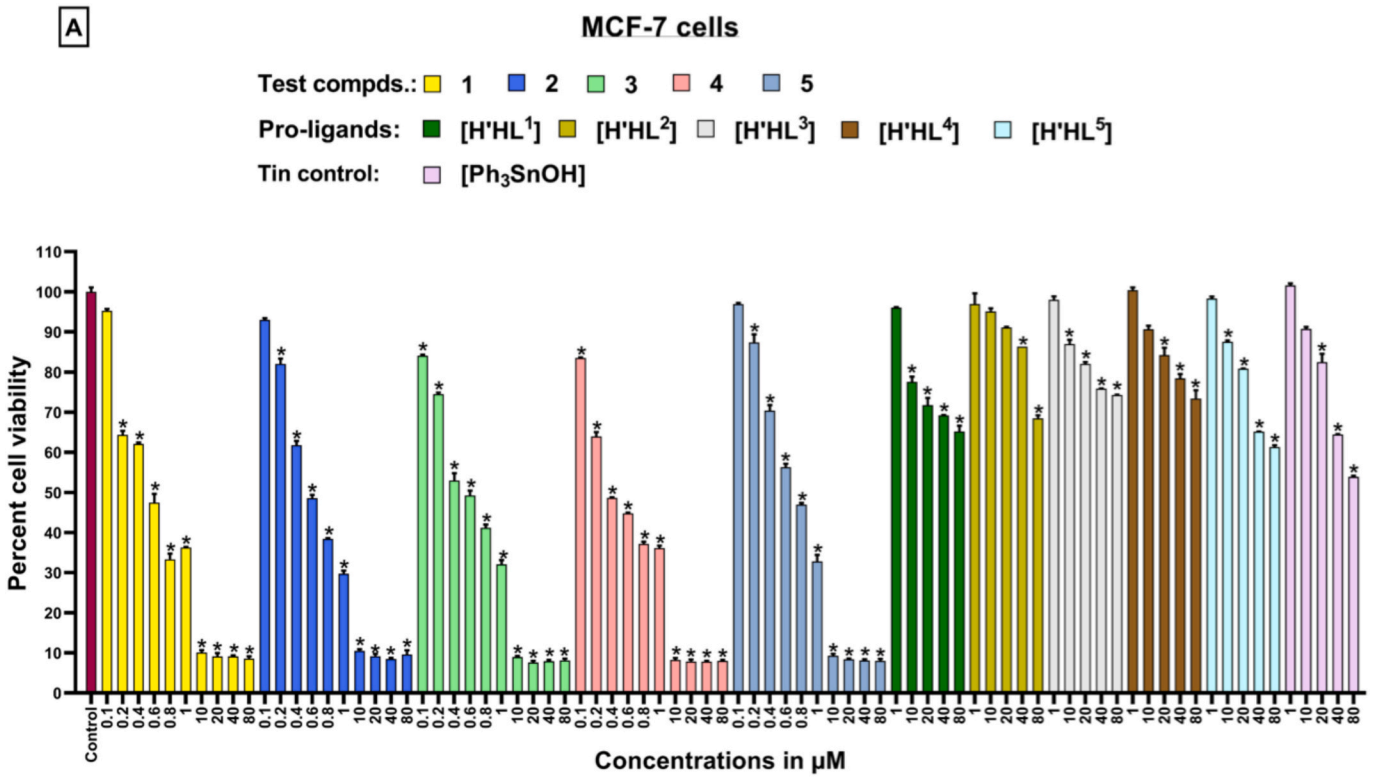

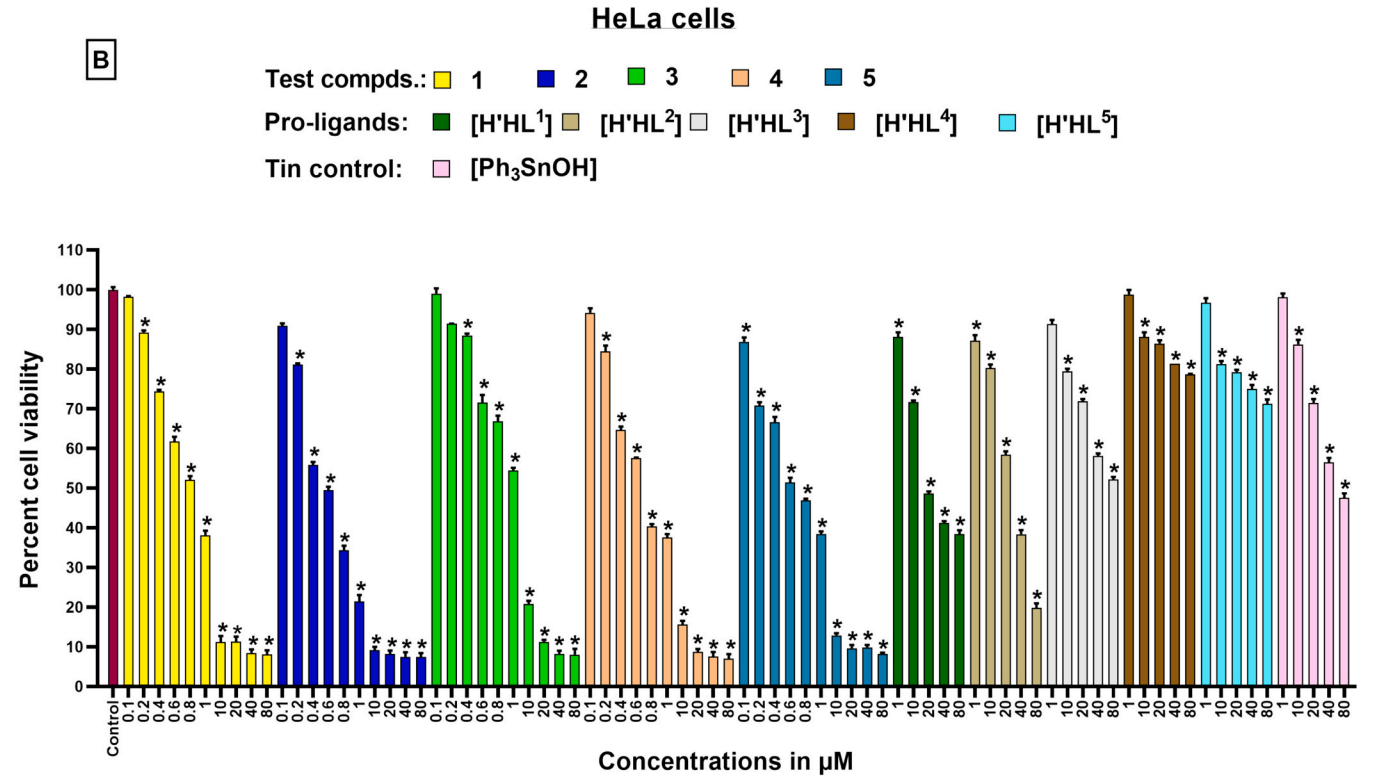

Fig. 4. Dose-dependent anti-proliferative effects (MTT assay) of treated (A) MCF-7 cancer cells and (B) HeLa cancer cells at the variable concentrations of test compounds **1**–**5**, the pro-ligands (H′HL^1, H′HL^2, H′HL^3, H′HL^4 and H′HL^5), and tin control reference compound Ph_3SnOH. (C) MTT assay of the treated HEK-293 normal cells at different concentrations of compound **4** and its pro-ligand H′HL^4. In comparison to the control, $^*p < 0.05$ is considered statistically significant.

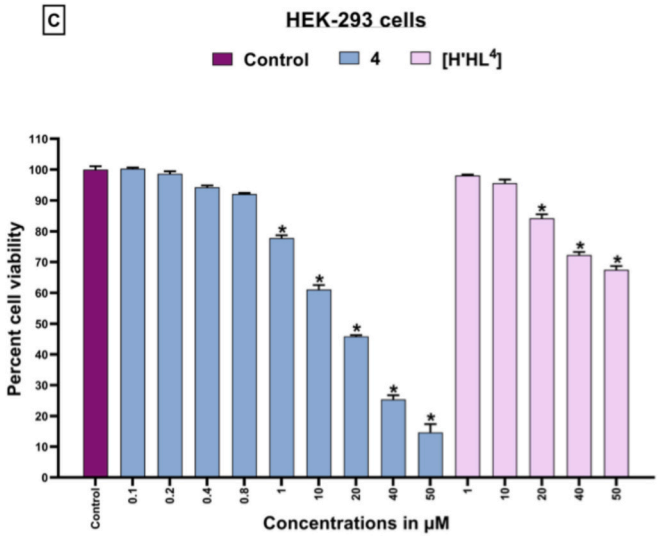

Fig. 4. (*continued*).

Table 4
The cytotoxicity (IC_{50} values) of the investigated compounds (triphenyltin(IV) compounds **1**–**5**, pro-ligands along with organotin(IV) precursor, Ph_3SnOH) against cancer cells (MCF-7 and HeLa) and normal cells (HEK-293).

Compounds	IC_{50} (μM) ± SEM[a] after 24 h of cells incubation		
	MCF-7 cells	HeLa cells	HEK-293 cells
Triphenyltin test compounds (**1**–**5**) and pro-ligands (H_2L)			
1	0.54 ± 0.27	0.60 ± 0.11	–
2	0.60 ± 0.14	0.60 ± 0.19	–
3	0.60 ± 0.27	0.73 ± 0.13	–
4	0.40 ± 0.16	0.60 ± 0.21	18 ± 0.11
5	0.78 ± 0.10	1.70 ± 0.23	–
H′HL[1]	>80	18 ± 0.54	–
H′HL[2]	>80	>80	–
H′HL[3]	>80	>80	–
H′HL[4]	>80	>80	>50
H′HL[5]	>80	>80	–
Organotin controls and standard drug			
Ph_3SnOH	>80	61 ± 0.89	–
CDDP	30 ± 0.35	30 ± 0.35	

[a] SEM; Standard error of mean calculated for the average of three sets of independent experiments.

−20 °C. After centrifugation, the cells were stained with 20 μg/mL PI, 100 μg/mL RNase A, and 0.1 % triton-X in phosphate-buffered saline, followed by a 30 min incubation at 37 °C.

2.6.7. Statistical analysis

The results have been presented as SEM in triplicate. Analysis of variance (ANOVA) and Tukey's post-hoc test were performed utilizing GraphPad Prism 8.0.2 Software. These analyses were carried out with a 95 % confidence level, with statistical significance defined as a *p*-value of <0.05. Statistical significance levels were denoted by ns, *, **, ***, and **** for *p*-values of <0.05, <0.01, <0.001, and <0.0001, respectively.

3. Results and discussion

3.1. Design aspects, synthesis and spectroscopic characterization

The pro-ligands H′HL[3] to H′HL[5] were synthesized using standard diazo-coupling reaction. This reaction involved aryldiazonium chloride, generated from 2-trifluoromethyl aniline, 3-trifluoromethyl aniline, or 4-trifluoromethyl aniline, and salicylic acid in an alkaline solution under cold conditions. For comparison, we also synthesized H′HL[1] and H′HL[2] from aniline and 4-fluoroaniline, following the procedures outlined in previous studies [35,47,48]. Five triphenyltin(IV) 2-hydroxy-5-(phenyldiazenyl)benzoates with the general formula [Ph_3Sn(HL)] were synthesized in reasonable yields (55–64 %) from triphenyltin hydroxide and the corresponding pro-ligands (H′HL[1] to H′HL[5]) in anhydrous toluene as outlined in Scheme 1.

The compounds **1**–**5** are orange crystalline solids with distinct melting points, showing notable stability in both their solid state and when dissolved in solution, as evidenced by SC-XRD analysis, ^{119}Sn NMR, and electronic spectral studies. Diagnostically useful FT-IR absorptions are compiled in the Experimental section, while FT-IR spectra of pro-ligands (H′HL[1] to H′HL[5]), and triphenyltin(IV) compounds **1**–**5** are presented in ESI Figs. S4–S13. The FT-IR spectral data of the compounds **1**–**5** were compared to those of the pro-ligands, and the corresponding vibrations were analyzed to assess the coordination behavior of the carboxylic group. The pro-ligands display a strong absorption band in the range of 1661–1668 cm^{-1}, assigned to ν(COOH), which is absent in triphenyltin compounds **1**–**5**. This indicates the deprotonation of the carboxylic acid group due to complexation. The FT-IR spectra of compounds **1**–**5** show two bands at approximately 1634 cm^{-1} and 1390 cm^{-1}, which correspond to the asymmetric (ν_{as}) and symmetric (ν_s) vibration frequencies of the COO^- group, respectively. The $\Delta\nu$ value ($\Delta\nu = \nu_{as}(COO) - \nu_s(COO)$) for these compounds ranges from 236 to 248 cm^{-1}, indicating a monodentate coordination mode for the carboxylate ligand [51]. This finding aligns with the established range for monodentate coordination ($\Delta\nu \geq 200$ cm^{-1}), but it also suggests a borderline case for chelating bidentate or anisobidentate coordination modes of the carboxylate ligand [51]. This ambiguity was ultimately clarified through X-ray single-crystal analysis of compounds **1**–**5** (vide infra). The IR spectra of compounds **1**–**5** also exhibited characteristic bands in the range of 695–698 cm^{-1}, corresponding to ν(Sn—C), when compared to the spectra of the respective pro-ligands [52]. The pro-ligands and compounds **1**–**5** were also studied in solution using NMR spectroscopy (ESI Figs. S14–S45). In general, the pro-ligands did not exhibit proton signal for the carboxylic acid, except for H′HL[2], which may be attributed to possible exchange due to the presence of water in the solvent. However, both pro-ligands and triphenyltin compounds **1**–**5** displayed a singlet assigned to OH in the range of 10.9 to 11.9 ppm. The ^{1}H and ^{13}C NMR spectra of compounds **1**–**5** in $CDCl_3$ exhibit distinctive signal patterns in the aromatic regions of the ligand and the SnPh groups, (Ph-2 (*ortho*- protons: 7.74–7.82 ppm); and Ph-3 and Ph-4 (*meta*- and *para*-

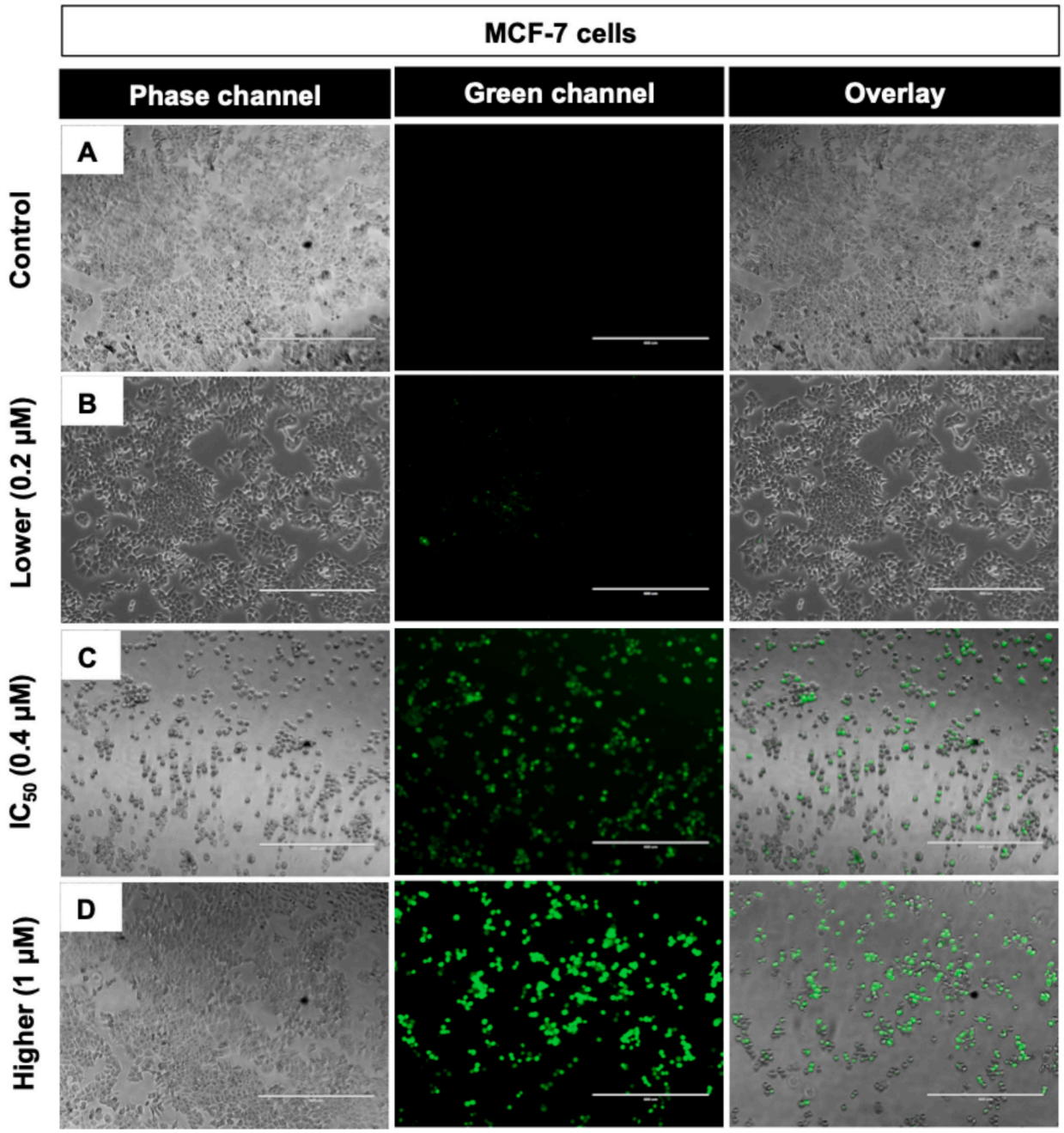

Fig. 5. Intracellular ROS detection in control and test compound **4** exposed to MCF-7 cells at different concentrations for 24 h. Using the DCFH-DA fluorescent labeling method, intracellular ROS levels were measured. Microscope images showing increased intracellular ROS level under different treatment conditions (A) Control (B) Lower concentration (0.2 μM) (C) IC_{50} concentration (0.4 μM) (D) Higher concentration (1 μM).

protons: 7.43–7.53 ppm)) including the $^{117/119}$Sn coupling patterns. In the ^{13}C NMR spectra of the triphenyltin(IV) derivatives **1**–**5**, the carboxylic carbon is observed at a downfield position compared to that of the corresponding free pro-ligand. This downfield shift confirms the coordination of the carboxylate oxygen to the Sn atom. The signals for the aromatic carbon, —CF_3 groups, and Ph_3Sn (Ph-1 to Ph-4: *ipso-*, *ortho-*, *meta-* and *para-* carbon atoms) appeared in their anticipated regions. The ^{19}F NMR spectra for the pro-ligands H′HL^2 to H′HL^5 exhibit distinct signals at δ −109.6, −56.8, − 61.99, and −62.5 ppm, respectively, when dissolved in $CDCl_3$. These signals remain unchanged in their triphenyltin compounds **2**–**5**. The chemical shifts and $^1J(^{13}C\text{-}^{119}Sn)$ coupling constants for four-coordinate triphenyltin(IV) complexes are typically found between −40 and −120 ppm and between 550 and 660 Hz. In contrast, five-coordinate compounds with a trigonal bipyramidal geometry and equatorial phenyl groups exhibit shifts ranging from −180 to −260 ppm, with coupling constants between 750 and 850 Hz [53]. In the present investigation, the ^{119}Sn NMR spectra of triphenyltin(IV) derivatives **1**–**5** in $CDCl_3$ showed singlets at δ −88.8, −88.1, −90.3, −90.9, and −86.8 ppm, respectively. These values are consistent with those typically observed for tetrahedral tin compounds in solution [53]. Insufficient signal-to-noise prevented observation of $^1J(^{13}C\text{-}^{119}Sn)$ coupling constants, although $^2J(^{13}C\text{-}^{119}Sn)$, $^3J(^{13}C\text{-}^{119}Sn)$ and $^4J(^{13}C\text{-}^{119}Sn)$ were observed in most cases. Compounds **1**–**5** were also characterized by HRMS, and the mass-to-charge ratios of the ions were measured in an acetonitrile solution within the range of *m/z* 100–1200 Da. The most relevant mass clusters detected in the experiments are shown in the ESI

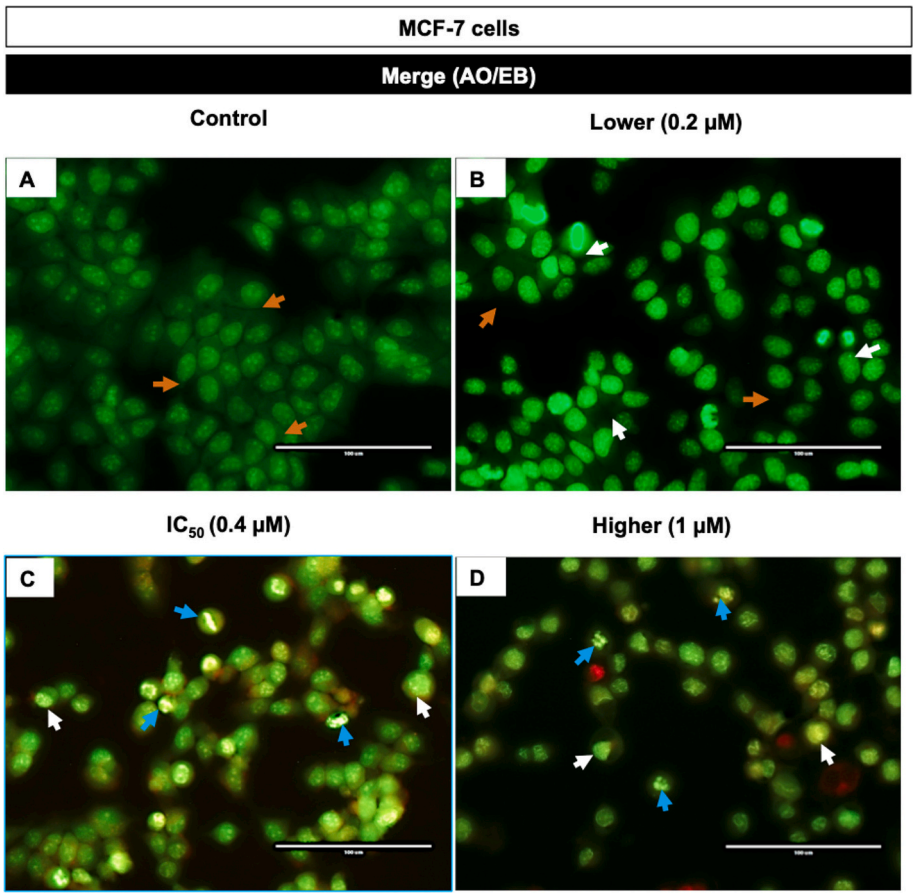

Fig. 6. Microscope images showing increased intracellular ROS level under different treatment conditions (A) Control (B) Lower concentration (0.2 μM) (C) IC_{50} concentration (0.4 μM) (D) Higher concentration (1 μM). The brown, white and blue arrows represent the live, early apoptotic and late apoptotic cells, respectively. (For interpretation of the references to color in this figure legend, the reader is referred to the web version of this article.)

Figs. S46–S50. In the mass spectra of compounds **1**–**5**, a weak molecular ion peak corresponding to the protonated molecule $[M + H]^+$ was observed, with m/z values of 593.1786 (0.20 %) for **1**, 611.0157 (1.96 %) for **2**, 661.0024 (0.57 %) for **3**, 661.0152 (0.17 %) for **4**, and 661.0437 (0.27 %) for **5**. The fragmentation patterns of all five compounds also display a characteristic high-intensity peak at m/z = 351 (>86 %) for $[Ph_3Sn]^+$, which results from the loss of one mole of ligand from the complex, involving the cleavage of a weak Sn—O bond [54]. The mass spectrometric analysis also provided valuable insights. Compounds **2**–**5**, which contain fluorine atoms, consistently exhibited a prominent peak at m/z = 745 (>92 %), corresponds to the $[C_{31}H_{19}F_2N_2O_3Sn_2]^+$ fragment. which could not be assigned. This feature was not observed in compound **1**, which lacks fluorine.

3.2. Description of the solid-state structures

The X-ray crystal structures of the pro-ligand $H'HL^5$ (Fig. 1a) and the complexes **3**, **4**, and **5** (Fig. 1b–d) were determined using single-crystal X-ray diffraction. Crystallographic data and structure refinement statistics are provided in ESI Table S1. The following comparison underscores the structural consistency across the ligands while highlighting differences in CF_3 group positioning, torsion angles, dihedrals, and supramolecular interactions. Structurally, the pro-ligand $H'HL^5$ and its ligated form (HL^5) in compound **5** differ from the ligands in **3** and **4** by the position of the CF_3 group on the trifluoromethylphenyl ring: *para* (4-position) in $H'HL^5$ and **5**, *ortho* (2-position) in **3**, and *meta* (3-position) in **4**. Aside from this distinction, the ligands HL^3, HL^4, HL^5, and pro-ligand $H'HL^5$ share remarkably similar structural features. Specifically, the trifluoromethylphenyl and 2-hydroxybenzoate rings are *trans* across the diazenyl linker in each case, and an S(6) *intra*-molecular O3-H3…O2 hydrogen bond motif [55] is consistently observed within the 2-hydroxybenzoate group.

The structural similarities are highlighted in a least-squares overlay of atoms O1–O3, N1, N2, C1–C8 (Fig. 2). Quantitative details, including interatomic distances, angles, torsions, and dihedrals, are summarized in Tables 1 and 2. These data confirm the general correlation between the 2-hydroxy-5-diazenylbenzoate fragments across all structures. However, the relationship between the trifluoromethylphenyl and 2-hydroxybenzoate rings differs notably for compound **5**, which exhibits a dihedral of 40.36(19)°, being significantly larger than those observed in $H'HL^5$, **3A**, **3B**, and **4**, which range from 4.48(16)° to 9.87(12)° (Table B). Additionally, the trifluoromethylphenyl rings in **3A** and **3B** are flipped by approximately 180° compared to that in **4** relative to the diazenyl linkage (Fig. 2).

In complexes **3**, **4**, and **5**, the Sn1 atom bonds to three phenyl groups (Sn1-C15, Sn1-C21, Sn1-C27) and forms one short bond (Sn1-O1 are in the range 2.0654(16)–2.145(4) Å) and one much longer interaction (Sn1-O2 range from 2.7535(11)–3.012(4) Å). Thus, the geometry at Sn1 may be classified as either 4-coordinate or 5-coordinate. For the former case, the Sn1 geometries are best described as distorted tetrahedral, as τ_4 parameters [56] range from 0.81 for the major disorder component in **5** to 0.91 in **4** (ideal values being 1 for perfect tetrahedral and 0 for square planar). If Sn1 is taken as 5-coordinate, then the geometry is distorted face-capped tetrahedral.

These distortions, influenced by the carboxylate group O2 atom, are reflected in the angles subtended at the Sn1 atom. For example, the O1-Sn1-C15 angles are consistently smaller (93.94(5)° to 95.38(8)°) than the ideal tetrahedral angle of 109.5° (Table 2). Notably, the $SnPh_3$ group

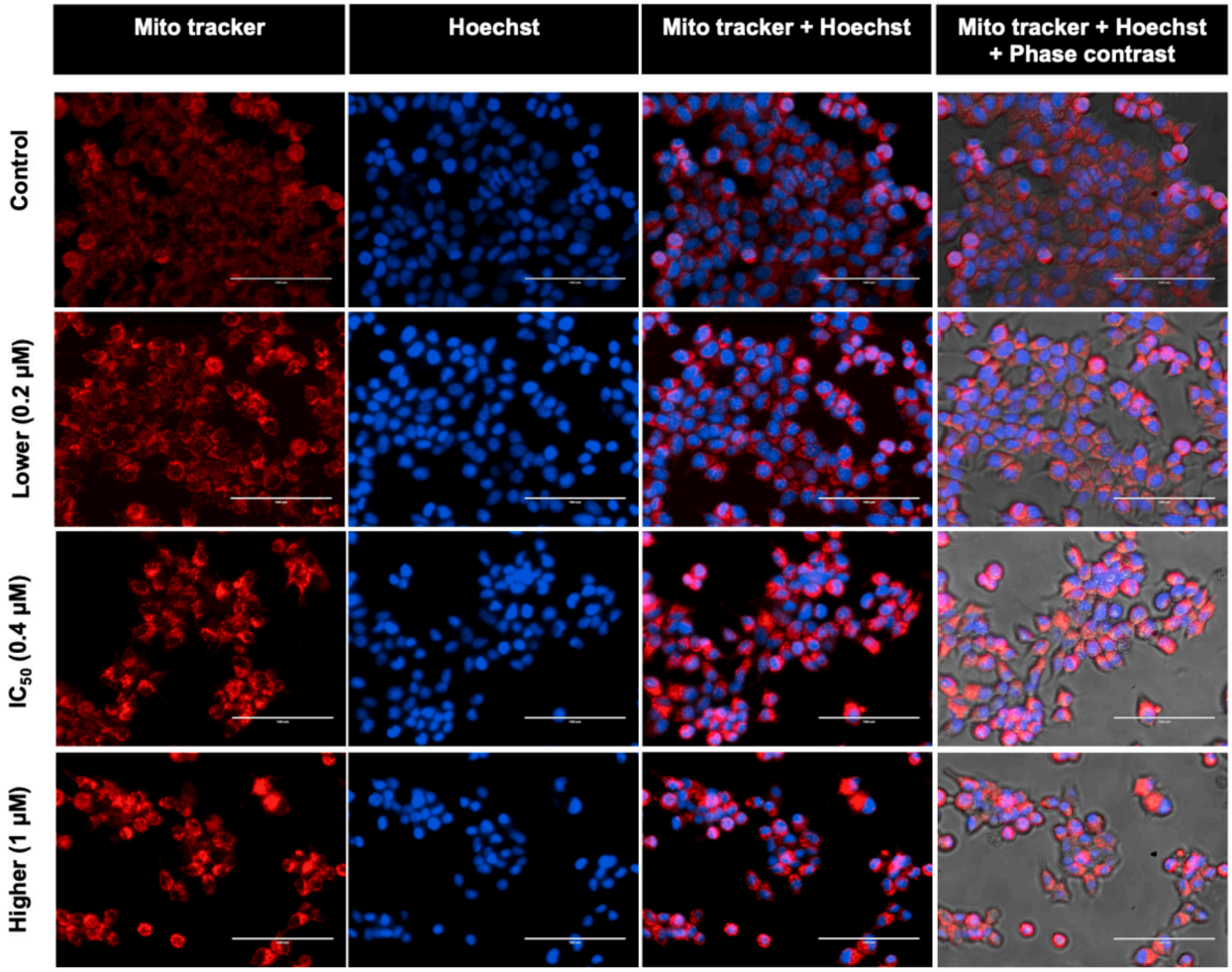

Fig. 7. Detection of mitochondrial distribution in control and treated MCF-7 cells using Mito Tracker red with varying concentrations of compound **4**. The increment in the mitochondrial delocalization has been observed with respect to the increase in concentrations. (For interpretation of the references to color in this figure legend, the reader is referred to the web version of this article.)

in compound **5** is extensively disordered, resulting in reduced geometric precision relative to **3** and **4**.

The pro-ligand $H'HL^5$ uniquely forms an *inter*molecular hydrogen bond (O1—H1…O2^{inv}, where *inv* = 1-*x*, 2-*y*, 2-*z*; Fig. 3a). In contrast, the absence of suitable H-bond donors in **3**, **4**, and **5** precludes any strong *inter*-molecular hydrogen bonding. These structures exhibit only weak O—H…F (in $H'HL^5$ and **5**) and C-H…F (in $H'HL^5$ and **4**) contacts, which are of limited structural significance. Supramolecular interactions include π…π [57] stacking and C—H…π [58] contacts. In $H'HL^5$, inversion-related molecules (1-*x*, 1-*y*, 1-*z*) form dimers via π…π stacking (Fig. 3a). In **3**, each independent molecule forms inversion-related dimers via (−*x*, −*y*, −*z*) for **3A** and (1-*x*, −*y*, 1-*z*) for **3B** (Fig. 3b). In **4**, C19-H19…π interactions between inversion (1-*x*, 1-*y*, 1-*z*) related molecules create loose dimeric motifs (Fig. 3c). Finally, in **5**, π…π overlap occurs between benzoate rings of 4_2-screw-related molecules (via 0.5-*x*, 1.5-*y*, *z*; Fig. 3d). These details are summarized in Table 3. Despite the similarities in molecular structure for these compounds, their crystal packing arrangements are markedly different.

3.3. Anti-proliferative effects, mechanism of cell death, and generation of reactive oxygen species

3.3.1. Assessment of concentrations that influence cell survival

In the current study, the MTT assay was performed on MCF-7 and HeLa cancer cells, as well as normal (healthy) HEK-293 cells, to assess the *in vitro* anticancer properties and cytotoxicity of test compounds **1**–**5**. These results were compared to those of the respective pro-ligands ($H'HL^1$, $H'HL^2$, $H'HL^3$, $H'HL^4$, and $H'HL^5$), the reference compound (Ph_3SnOH), and untreated controls after 24 h of treatment. The chemotherapy drug CDDP was used as a positive control in all experiments. Among the cancer cell tested, compounds **1**–**5** exhibited high cytotoxicity in MCF-7 cells (Fig. 4A) compared to HeLa cells (Fig. 4B), and cell viability decreased in a concentration-dependent manner. The IC_{50} values are presented in Table 4. Among the compounds tested, compound **4** ($[Ph_3Sn(HL^4)]$) showed the highest cytotoxicity in MCF-7 cells. The IC_{50} value of compound **4** was found to be 0.4 μM, which is comparatively lower than that of the other tested compounds (Fig. 4A). HEK-293 cells treated with compound **4** showed 94 % cell viability at the IC_{50} concentration, suggesting its non-toxicity toward normal cells (Fig. 4C). The cytotoxicity of the pro-ligands ($H'HL^1$, $H'HL^2$, $H'HL^3$, $H'HL^4$, and $H'HL^5$) and the tin control Ph_3SnOH was found to be considerably lower compared to the compounds. The percent cell viability of MCF-7 cells was higher when treated with various concentrations of the pro-ligands and tin control Ph_3SnOH, indicating that the pro-ligands alone were less cytotoxic. Therefore, based on these results, it can be concluded that the cytotoxic efficacy of compound **4** is significantly higher in MCF-7 cells compared to the other compounds, with no aggressive cytotoxicity observed in normal HEK-293 cells. Hence, compound **4** could be a promising candidate for further development as a potential treatment for breast cancer.

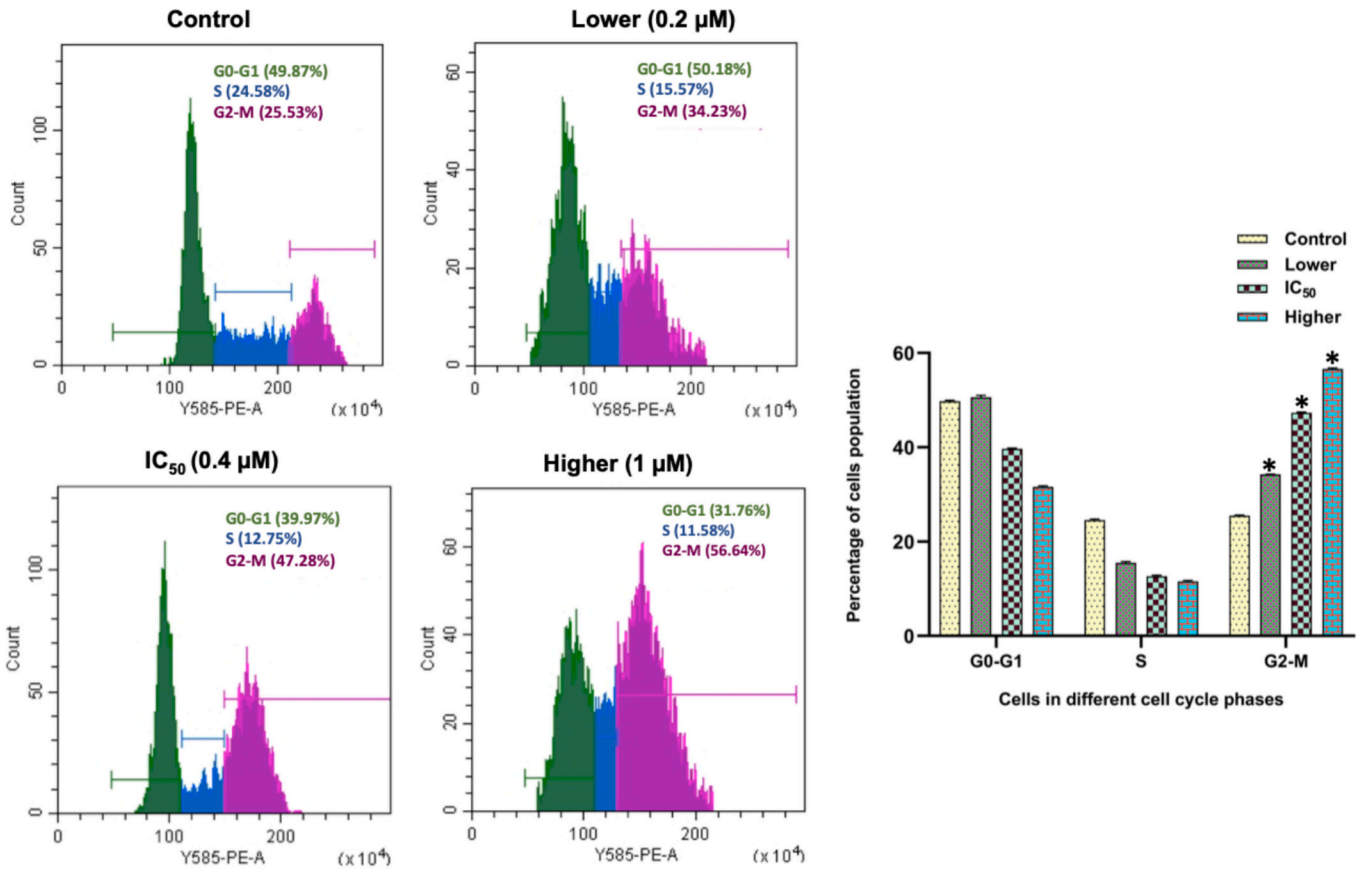

Fig. 8. Cell cycle analysis of the control and exposed MCF-7 cells with various concentrations of compound **4**. The cells arrest at the different cell cycle phases has been analyzed using the flow cytometry. Statistical significance in relation to the cell cycle phase control was denoted by $*p < 0.05$.

3.3.2. In vitro generation of reactive oxygen species (ROS)

The generation of reactive oxygen species (ROS) in MCF-7 cells induced by compound **4** was investigated using the DCFH-DA dye. DCFH-DA is a non-fluorescent probe that oxidizes in the presence of peroxides and free radicals inside cells, producing the fluorescent compound DCF, which becomes trapped within the cells [59]. This method is widely used and considered the most convenient for detecting intracellular ROS generation.

Our results show an increase in ROS generation as the concentration of compound **4** increases (Fig. 5). A significant increase in ROS levels, compared to the control, was observed in cells treated with IC_{50} (0.4 μM) and higher (1 μM) concentrations of compound **4**. No significant ROS production was observed in cells treated with the lower concentration (0.2 μM). These findings indicate that compound **4** is effective at initiating ROS production above its threshold, thereby converting the non-fluorescent DCFH-DA into fluorescent DCF. Such a generation of ROS levels induced by phenyltin compounds in cancer cells has been noted earlier [60,61].

3.3.3. Evaluation of cellular and nuclear morphological alterations during apoptosis

The induction of apoptosis through AO/EB staining was analyzed, and the images are displayed in Fig. 6. The uniform distribution of AO staining (green) was observed in the untreated control cells, indicating their live and healthy condition. The early apoptotic cells exhibited bright green fluorescence with condensed nuclei, but no significant changes relative to the control were observed with the lower concentration (0.2 μM) of compound **4**. In contrast, cells treated with the IC_{50} (0.4 μM) and higher concentrations (1 μM) revealed both early and late apoptotic features, such as compromised cellular membranes and nuclear disintegration. These cells incorporated both AO and EB stains and appeared yellow. Previous studies have demonstrated that organotin derivatives induce cell shrinkage, chromatin condensation, and membrane blabbing in breast cancer cells [62]. These compounds are believed to interact with DNA, potentially disrupting replication and transcription, leading to cell death and apoptosis [63]. Therefore, the evidence suggests that compound **4** promotes apoptosis in MCF-7 cells in a dose-dependent manner.

3.3.4. Analysis of mitochondrial distribution patterns

The mitochondrial aggregation pattern before apoptosis was analyzed using Mitotracker Red and Hoechst staining. Mitotracker Red was primarily used to visualize the localization of cytoplasmic mitochondria within the cells, while Hoechst served as a counterstain to highlight the nucleus. Treated MCF-7 cells, exposed to different concentrations of compound **4**, showed changes in the mitochondrial distribution pattern, indicating the progression of apoptosis. At a lower concentration (0.2 μM), mitochondrial aggregation was observed, characterized by a bright red color surrounding the nucleus. This aggregation became more prominent at concentrations of 0.4 μM and 1 μM (Fig. 7). These results suggest that compound **4** induces mitochondrial redistribution, thereby promoting apoptosis. Studies on organotin derivatives have shown their potential to interfere with mitochondrial function and induce mitochondrial-mediated apoptosis [64]. Our findings further suggest that compound **4** not only promotes mitochondrial aggregation at the periphery of the nucleus but also influences regulation of the apoptosis pathway.

3.3.5. Cell cycle analysis

To assess the distribution of cell cycle stages, MCF-7 cells were treated with compound **4** for 24 h. Flow cytometry analysis was performed on PI-stained MCF-7 cells to examine DNA content following

exposure to varying concentrations of compound **4** (Fig. 8). MCF-7 cells at various stages of the cell cycle were analyzed for DNA content after treatment with compound **4**. Cells exposed to a range of compound **4** concentrations (0.2 μM, 0.4 μM, and 1 μM) exhibited a concentration-dependent cell cycle arrest. At the 0.2 μM concentration, a notable increase in cell arrest was observed compared to the control, with an 8.7 % increase in arrested cells. Similarly, cells treated with 0.4 μM and 1 μM concentrations also displayed significant cell cycle arrest, with increases of 21.75 % and 31.11 %, respectively. These findings suggest that compound **4** effectively induces cell cycle arrest, which may subsequently promote apoptosis. Previous studies involving organotin(IV) compounds have shown that they can induce G2/M phase arrest in various cancer cells [23,64].

4. Conclusions

This study focuses on the preparation and characterization of a series of novel triphenyltin(IV) derivatives with fluoro-substituted arylazosalicylic acids ($H'HL^2$, $H'HL^3$, $H'HL^4$, and $H'HL^5$), alongside the non-fluorinated pro-ligand $H'HL^1$ for comparison. Compounds **3**–**5** were characterized using single-crystal X-ray diffraction (SCXRD) and various spectroscopic and analytical techniques. X-ray diffraction analysis revealed a distorted tetrahedral configuration, with the carboxylate ligand coordinating in a monodentate manner. Additionally, ^{119}Sn NMR spectroscopic studies confirmed that the tin complexes maintain their solid-state structures in deuterated chloroform. Compounds **1**–**5** were evaluated *in vitro* for their antiproliferative activity against MCF-7 (human breast cancer) and HeLa (human cervical cancer) cells. The IC_{50} values for the triphenyltin(IV) compounds ranged from 0.40 to 0.78 μM for MCF-7 cells, compared to 0.60 to 1.70 μM for HeLa cells. Notably, among the fluorinated triphenyltin compounds **2**–**5**, [$Ph_3Sn(HL^4)$] (compound **4**), whose ligand contains a 3′-CF_3 group, demonstrated the highest cytotoxicity against MCF-7 cells, with an IC_{50} of 0.40 ± 0.16 μM, while exhibiting minimal cytotoxicity to normal cells. The triphenyltin(IV) compounds exhibited favorable cell bioavailability and accumulation, characteristic of lipophilic substances. In conclusion, [$Ph_3Sn(HL^4)$] **4** stands out as a novel and promising candidate for antiproliferative drug development, warranting further investigation.

CRediT authorship contribution statement

Tushar S. Basu Baul: Writing – review & editing, Writing – original draft, Supervision, Resources, Project administration, Methodology, Investigation, Formal analysis, Conceptualization. **Amon Das:** Validation, Software, Methodology, Investigation, Data curation. **Rupen Tamang:** Validation, Methodology, Investigation, Formal analysis, Data curation. **Andrew Duthie:** Writing – review & editing, Resources, Investigation, Formal analysis, Data curation. **Biplob Koch:** Writing – review & editing, Supervision, Resources, Project administration, Methodology, Formal analysis. **Sean Parkin:** Writing – review & editing, Validation, Software, Resources, Investigation, Funding acquisition, Formal analysis, Data curation.

Declaration of competing interest

The authors declare no conflict of interest.

Acknowledgements

AD thanks University Grants Commission, New Delhi for the award of non-NET fellowships. Authors (TSBB and AD) thank SAIF-NEHU, Shillong for providing NMR measurements and the DST-FIST program (No. SR/FST/CS-II/2019/99(C)), Government of India, for providing the HRMS instrument to the Department of Chemistry, NEHU, Shillong. Deakin University's Advanced Characterization Facility is acknowledged for use of the NMR instrumentation. SP thanks the US NSF MRI program (grant CHE-1625732). BK acknowledges Banaras Hindu University for providing funding under the IoE scheme (File No. R/Dev/D/IoE/Incentive/2021-22/32449).

Appendix B. Supplementary data

CCDC 2410397-2410400 contain the supplementary crystallographic data for compounds$H'HL^5$ and **3**–**5** reported in this paper. These data can be obtained free of charge via http://www.ccdc.cam.ac.uk/conts/retrieving.html, or from the Cambridge Crystallographic Data Center, 12 Union Road, Cambridge CB2 1EZ, UK; fax: (+44) 1223-336-033; or e-mail: deposit@ccdc.cam.ac.uk.

Electronic Supplementary Information (ESI) available: UV–Vis absorption spectra (Figs. S1 and S2); Stability study (Fig. S3); FT-IR (ATR) spectra (Figs. S4–S13), NMR spectra (Figs. S14–S45) and HRMS spectra (Figs. S46–S50). Table with crystallographic details are included as supplementary material. Supplementary data to this article can be found online at https://doi.org/10.1016/j.jinorgbio.2025.112898.

Data availability

Data will be made available on request.

References

[1] H. Sung, J. Ferlay, R.L. Siegel, M. Laversanne, I. Soerjomataram, A. Jemal, F. Bray, Global cancer statistics 2020: GLOBOCAN estimates of incidence and mortality worldwide for 36 cancers in 185 countries, CA-Cancer J. Clin. 71 (2021) 209–249.
[2] K. Ding, X. Liu, L. Wang, L. Zou, X. Jiang, A. Li, J. Zhou, Targeting JWA for cancer therapy: functions, mechanisms and drug discovery, Cancers 14 (2022) 4655.
[3] S. Dasari, P.B. Tchounwou, Cisplatin in cancer therapy: molecular mechanisms of action, Eur. J. Pharmacol. 740 (2014) 364–378.
[4] N. Martinho, T.C.B. Santos, H.F. Florindo, L.C. Silva, Cisplatin-membrane interactions and their influence on platinum complexes activity and toxicity, Front. Physiol. 9 (2019) 1898.
[5] M. Kartalou, J.M. Essigmann, Mechanisms of resistance to cisplatin, Mutat. Res. Fundam. Mol. Mech. Mutagen. 478 (2001) 23–43.
[6] L. Galluzzi, I. Vitale, J. Michels, C. Brenner, G. Szabadkai, A. Harel-Bellan, M. Castedo, G. Kroemer, Systems biology of cisplatin resistance: past, present, and future, Cell Death Dis. 5 (2014) e1257.
[7] Cisplatin Side Effects: Common, Severe, Long Term, Drugs.Com.; https://www.drugs.com/sfx/cisplatin-side-effects.html (updated October 2024).
[8] M. Kumar, Z. Abbas, P. Siwach, J. Sharma, A. Rani, S. Sharma, P. Aggarwal, P.-L. Show, S. Haque, V. Garg, H.S. Tuli, J. Adv. Biotechnol. Exp. Ther. 6 (2023) 386–402.
[9] C.G. dos Santos, G.M. de Lima, Tin and organotin coordination polymers and covalently bonded supramolecular materials – the last 15 years of research, Coord. Chem. Rev. 410 (2020) 213236.
[10] P.A. Storozhenko, K.D. Magdeev, A.A. Grachev, N.I. Kirilina, V.I. Shiryaev, Organotin compounds in industrial catalysis, part 2: processes of polyurethane formation, Cat. Chem. Petrochem. Ind. 12 (2020) 304–315.
[11] R. Joshi, N. Tomar, S. Pokharia, I. Joshi, Recent advancements in organotin(IV) complexes of drugs: synthesis, characterization, and application, Results Chem. 5 (2023) 100955.
[12] S. Birara, A. Betal, P. Lama, S. Sahu, R.K. Metre, WORM type memory device based on ionic organotin complex using 1,5-diphenyl-3-(2-pyridyl)formazan ligand, J. Mol. Struct. 1287 (2023) 135708.
[13] A. Mishra, A. Betal, N. Pal, R. Kumar, P. Lama, S. Sahu, R. Metre, Molecular memory switching device based on a tetranuclear organotin sulfide cage $[(RSn^{IV})_4(\mu\text{-}S)_6]\cdot 2CHCl_3\cdot 4H_2O$ (R = 2-(Phenylazo)phenyl): synthesis, structure, DFT studies, and memristive behavior, ACS Appl. Electron. Mater. 2 (2020) 220–229.
[14] M.E. Sánchez Vergara, E. Gómez, E.T. Dircio, J.R.Á. Bada, S.C. Pérez, J.M. G. Hidalgo, A.G. Hernández, S.H. Ortega, Pentacoordinated organotin(iv) complexes as an alternative in the design of highly efficient optoelectronic and photovoltaic devices: synthesis and photophysical characterization, Int. J. Mol. Sci. 24 (2023) 5255.
[15] M.E. Sánchez-Vergara, L. Hamui, E. Gómez, G.M. Chans, J.M. Galván-Hidalgo, Design of promising heptacoordinated organotin(IV) complexes-PEDOT: PSS-based composite for new-generation optoelectronic devices applications, Polymers 13 (2021) 1023.
[16] C.R. Monzón-González, M.E. Sánchez-Vergara, W.E.V. Narváez, T. Rocha-Rinza, M. Hernández, E. Gómez, O. Jiménez-Sandoval, C. Álvarez-Toledano, Synthesis and characterization of organotin(IV) semiconductors and their applications in optoelectronics, J. Phys. Chem. Solid 150 (2021) 109840.
[17] T. Anasamy, C.F. Chee, L.V. Kiew, L.Y. Chung, In vivo antitumour properties of tribenzyltin carboxylates in a 4T1 murine metastatic mammary tumour model: enhanced efficacy by PLGA nanoparticles, Eur. J. Pharm. Sci. 142 (2020) 105140.

[18] M. Kumar, Z. Abbas, H.S. Tuli, A. Rani, Organotin complexes with promising therapeutic potential, Curr. Pharmacol. Rep. 6 (2020) 167–181.
[19] A.M. Cantón-Díaz, B.M. Muñoz-Flores, I. Moggio, E. Arias, A. de León, M.C. García-López, R. Santillán, M.E. Ochoa, V.M. Jiménez-Pérez, One-pot microwave-assisted synthesis of organotin Schiff bases: an optical and electrochemical study towards their effect in organic solar cells, New J. Chem. 42 (2018) 14586–14596.
[20] M. López-Espejel, A. Gómez-Treviño, B.M. Muñoz-Flores, M.A. Treto-Suarez, E. Schott, D. Páez-Hernández, X. Zarate, V.M. Jiménez-Pérez, Organotin Schiff bases as halofluorochromic dyes: green synthesis, chemio-photophysical characterization, DFT, and their fluorescent bioimaging in vitro, J. Mater. Chem. B 9 (2021) 7698–7712.
[21] R. Vinayak, D. Dey, D. Ghosh, D. Chattopadhyay, A. Ghosh, H.P. Nayek, Schiff base supported mononuclear organotin(IV) complexes: syntheses, structures and fluorescence cell imaging, Appl. Organomet. Chem. 32 (2018) e4122.
[22] N.Đ. Pantelić, Bojan Božić, B.B. Zmejkovski, N.R. Banjac, B. Dojčinović, L. A. Wessjohann, G.N. Kaluđerović, In vitro evaluation of antiproliferative properties of novel organotin(IV) carboxylate compounds with propanoic acid derivatives on a panel of human cancer cell lines, Molecules 26 (2021) 3199.
[23] C.N. Banti, S.K. Hadjikakou, T. Sismanoglu, N. Hadjiliadis, Anti-proliferative and antitumor activity of organotin(IV) compounds. An overview of the last decade and future perspectives, J. Inorg. Biochem. 194 (2019) 114–152.
[24] M. Sirajuddin, S. Ali, Organotin(IV) carboxylates as promising potential drug candidates in the field of cancer chemotherapy, Curr. Pharm. Des. 22 (2016) 6665–6681.
[25] A. Alama, B. Tasso, F. Novelli, F. Sparatore, Organometallic compounds in oncology: implications of novel organotins as antitumor agents, Drug Discov. Today 14 (2009) 500–508.
[26] V. Singh, N.K. Rana, M. Kashif, P.P. Manna, T.S. Basu Baul, Aqua-(2-formylbenzoato)triphenyltin(IV) induces cell cycle arrest and apoptosis in hypoxic triple negative breast cancer cells, Toxicol. In Vitro 86 (2023) 105484.
[27] M. Singh, N.K. Rana, M.S. Muthu, A. Jha, T.S. Basu Baul, B. Koch, Enhanced in vitro therapeutic efficacy of triphenyltin(IV) loaded vitamin E TPGS against breast cancer therapy, Mater. Today Commun. 31 (2022) 103256.
[28] M. Singh, V. Singh, T.S. Basu Baul, B. Koch, TPGS loaded triphenyltin(IV) micelles induced apoptosis by upregulating p53 in breast cancer cells and inhibit tumor progression in T-cell lymphoma bearing mice, Life Sci. 308 (2022) 120937.
[29] A.G. Davies, M. Gielen, K.H. Pannell, E.R.T. Tiekink, Tin Chemistry: Fundamentals, Frontiers, and Applications, Wiley, UK, 2008.
[30] R.G. Swisher, J.F. Vollano, V. Chandrasekhar, R.O. Day, R.R. Holmes, Inorg. Chem. 23 (1984) 3147–3152.
[31] J.F. Vallano, R.O. Day, D.N. Rau, V. Chandrasekhar, R.R. Holmes, Pentacoordinated molecules. 55. Intramolecularly formed pentacoordinated structures of triphenyltin esters of salicylic acid, o-anisic acid, and p-methylthiobenzoic acid, Inorg. Chem. 23 (1984) 3153–3160.
[32] M. Gielen, R. Willem, M. Biesemans, M. Boualam, A. El Khloufi, D. de Vos, Exceptionally high in vitro antitumor activity of substituted triphenyltin benzoates including salicylates against a human mammary tumor, MCF-7, and a colon carcinoma, WiDr, Appl. Organomet. Chem. 6 (1992) 287.
[33] T.S. Basu Baul, W. Rynjhah, X. Song, G. Eng, A. Linden, Synthesis, spectra, and crystal structures of the triorganotin(IV) 5-[(E)-2-(4-methylphenyl)-1-diazenyl]-2-hydroxybenzoates ($Me_3Sn\{O_2CC_6H_3$-p-OH[N=N(C_6H_4-4-CH_3)]$\}_n$, $Et_3Sn\{O_2CC_6H_3$-*p*-OH[N=N(C_6H_4-4-CH_3)]$\}OH_2$, and $Bz_3Sn\{O_2CC_6H_3$-*p*-OH[N=N(C_6H_4-4-CH_3)]$\}$, J. Organomet. Chem. 692 (2007) 3392–3399.
[34] T.S. Basu Baul, W. Rynjhah, E. Rivarola, A. Linden, Synthesis and characterization of triphenyltin(IV) 5-[(E)-2-(aryl)-1-diazenyl]-2-hydroxybenzoates. Crystal and molecular structures of $Ph_3Sn\{O_2CC_6H_3$-p-OH[N=N(C_6H_4-4-CH_3)]$\}$ and the 2,2′-bipyridine adduct $Ph_3Sn\{O_2CC_6H_3$-p-OH[N=N(C_6H_4-2-CH_3)]$\}OH_2\cdot C_{10}H_8N_2$, J. Organomet. Chem. 690 (2005) 613–621.
[35] T.S. Basu Baul, S. Dhar, S.M. Pyke, E.R.T. Tiekink, E. Rivarola, R. Butcher, F. E. Smith, Synthesis and characterization of triorganotin(IV) complexes of 5-[(E)-2-(aryl)-1-diazenyl]-2-hydroxybenzoic acids. Crystal and molecular structures of a series of triphenyltin 5-[(E)-2-(aryl)-1-diazenyl]-2-hydroxybenzoates (aryl = phenyl, 2-methylphenyl, 3-methylphenyl and 4-methoxyphenyl), J. Organomet. Chem. 633 (2001) 7–17.
[36] T.S. Basu Baul, S. Dhar, N. Kharbani, S.M. Pyke, R. Butcher, F.E. Smith, The synthesis and structural characterization of some triorganotin(IV) complexes of 5-(4-chlorophenylazo)salicylic acid: crystal and molecular structure of triphenyltin 5-(4-chlorophenylazo)salicylate, Main Group Met. Chem. 22 (1999) 413–421.
[37] T.S. Basu Baul, A. Das, S. Das Pramanik, P. Roy, A. Duthie, S. Parkin, Structural dynamics and evaluation of anti-proliferative effects of di-n-butyltin and triphenyltin fluoroazosalicylates on DU-145 prostate cancer cells, J. Mol. Struct. 1325 (2025) 140973.
[38] T.S. Basu Baul, R. Manne, E.R.T. Tiekink, Mono- and di-anionic coordination modes of arylazosalicylates in their bis(η^5-cyclopentadienyl)titanium(IV) complexes: syntheses and crystal structures, Inorg. Chim. Acta 484 (2019) 469–480.
[39] S. Parkin, H. Hope, Macromolecular cryocrystallography: cooling, mounting, storage and transportation of crystals, J. Appl. Cryst. 31 (1998) 945–953.
[40] Bruker-AXS, APEX5, SMART, SAINT, Bruker AXS Inc, Madison, Wisconsin, USA, 2023.
[41] L. Krause, R. Herbst-Irmer, G.M. Sheldrick, D. Stalke, Comparison of silver and molybdenum microfocus X-ray sources for single-crystal structure determination, J. Appl. Cryst. 48 (2015) 3–10.
[42] S. Parkin, B. Moezzi, H. Hope, XABS2: an empirical absorption correction program, J. Appl. Cryst. 28 (1995) 53–56.
[43] G.M. Sheldrick, SHELXT – integrated space-group and crystal-structure determination, Acta Crystallogr. A71 (2015) 3–8.
[44] G.M. Sheldrick, SHELXL – crystal structure refinement with SHELXL, Acta Crystallogr. C71 (2015) 3–8.
[45] A.L. Spek, checkCIF validation ALERTS: what they mean and how to respond, Acta Crystallogr. E76 (2015) 1–11.
[46] S. Parkin, Expansion of scalar validation criteria to three dimensions: the R-tensor, Acta Crystallogr. A56 (2000) 157–162.
[47] T.S. Basu Baul, B. Hlychho, S. Das Pramanik, A. Lyčka, P. Roy, A.G. Mahmoud, M.F. C. Guedes da Silva, Organotin(IV) complexes derived from 2,6-diacetylpyridine bis (2-hydroxybenzoylhydrazone) as prospective anti-proliferative agents: synthesis, characterization, structures and in vitro anticancer activity, J. Inorg. Biochem. 261 (2024) 112693.
[48] T. Mosmann, Rapid colorimetric assay for cellular growth and survival: application to proliferation and cytotoxicity assays, J. Immunol. Methods 65 (1983) 55–63.
[49] T.S. Basu Baul, I. Longkumer, A. Duthie, P. Singh, B. Koch, M.F.C. Guedes da Silva, Triphenylstannyl((arylimino)methyl)benzoates with selective potency that induce G1 and G2/M cell cycle arrest and trigger apoptosis via ROS in human cervical cancer cells, Dalton Trans. 47 (2018) 1993–2008.
[50] K. Neikirk, A.G. Marshall, B. Kula, N. Smith, S. LeBlanc, A. Hinton Jr., MitoTracker: a useful tool in need of better alternatives, Eur. J. Cell Biol. 102 (2023) 151371.
[51] (a) P.N. Nelson, R.A. Taylor, Theories and experimental investigations of the structural and thermotropic mesomorphic phase behaviors of metal carboxylates, Appl. Petrochem. Res. 4 (2014) 253–285;
(b) G.B. Deacon, R.J. Philips, Relationships between the carbon-oxygen stretching frequencies of carboxylato complexes and the type of carboxylate coordination, Coord. Chem. Rev. 33 (1980) 227–250.
[52] G.N. Kaluđerović, R. Paschke, S. Prashar, S. Gómez-Ruiz, Synthesis, characterization and biological studies of 1-D polymeric triphenyltin(IV) carboxylates, J. Organomet. Chem. 695 (2010) 1883–1890.
[53] J. Holeček, M. Nádvorník, K. Handlíř, A. Lyčka, ^{13}C and ^{119}Sn NMR study of some four- and five-coordinate triphenyltin(IV) compounds, J. Organomet. Chem. 241 (1983) 177–184.
[54] A. Lyčka, A. Růžička, J. Vaněček, L. Česlová, Structural study of di- and triorganotin(IV) dicarboxylates containing one double bond, J. Organomet. Chem. 695 (2010) 2493–2498.
[55] M.C. Etter, J.C. MacDonald, J. Bernstein, Graph-set analysis of hydrogen-bond patterns in organic crystals, Acta Crystallogr. B46 (1990) 256–262.
[56] L. Yang, D.R. Powell, R.P. Houser, Structural variation in copper(I) complexes with pyridylmethylamide ligands: structural analysis with a new four-coordinate geometry index, τ_4, Dalton Trans. (2007) 955–964.
[57] C. Janiak, A critical account on π–π stacking in metal complexes with aromatic nitrogen-containing ligands, J. Chem. Soc. Dalton Trans. (2000) 3885–3896.
[58] M. Nishio, The CH/π hydrogen bond in chemistry. Conformation, supramolecules, optical resolution and interactions involving carbohydrates, Phys. Chem. Chem. Phys. 13 (2011) 13873–13900.
[59] M. Whiteman, J.S. Armstrong, N.S. Cheung, J.-L. Siau, P. Rose, J.-T. Schantz, D. P. Jones, B. Halliwell, Peroxynitrite mediates calcium-dependent mitochondrial dysfunction and cell death via activation of calpains, FASEB J. 18 (2004) 1395–1397.
[60] M. Nath, M. Vats, P. Roy, Mode of action of tin-based anti-proliferative agents: biological studies of organotin(IV) derivatives of fatty acids, J. Photochem. Photobiol. B: Bio. 148 (2015) 88–100.
[61] S. Ali, S. Shahzadi, Imtiaz-ud-Din, Anticarcinogenicity and toxicity of organotin (IV) complexes: a review, Iran J. Sci. Technol. Trans. Sci. 42 (2018) 505–524.
[62] M.E.K. Stathopoulou, N. Zoupanou, C.N. Banti, A.P. Douvalis, C. Papachristodoulou, K.D. Marousis, G.A. Spyroulias, T. Mavromoustakos, S. K. Hadjikakou, Organotin derivatives of cholic acid induce apoptosis into breast cancer cells and interfere with mitochondrion; Synthesis, characterization and biological evaluation, Steroids 167 (2021) 108798.
[63] W. Jiang, Q. Qin, X. Xiao, Y. Tan, Diorganotin(IV) complexes based on tridentate ONO ligands as potential anticancer agents, J. Inorg. Biochem. 232 (2022) 111808.
[64] L. Yunlan, Z. Juan, L. Qingshan, Antitumor activity of di-n-butyl-(2,6-difluorobenzohydroxamato)tin(IV) against human gastric carcinoma SGC-7901 cells via G2/M cell cycle arrest and cell apoptosis, PloS One 9 (2014) e90793.